AD_____
(Leave blank)

Award Number: W81XWH-09-1-0004

TITLE: A Novel Hand-Held Optical Imager with Real-Time Co-registration Facilities toward Diagnostic Mammography

PRINCIPAL INVESTIGATOR:
Sarah Erickson

CONTRACTING ORGANIZATION:
Florida International University
Miami, FL 33199

REPORT DATE: January 2010

TYPE OF REPORT: Annual Summary

PREPARED FOR: U.S. Army Medical Research and Materiel Command
Fort Detrick, Maryland 21702-5012

DISTRIBUTION STATEMENT: (Check one)

■ Approved for public release; distribution unlimited

Distribution limited to U.S. Government agencies only; report contains proprietary information

REPORT DOCUMENTATION PAGE

Form Approved
OMB No. 0704-0188

1. REPORT DATE *(DD-MM-YYYY)*	2. REPORT TYPE	3. DATES COVERED *(From - To)*
01/31/10	Annual Summary	1 Jan 2009 – 31 Dec 2009

4. TITLE AND SUBTITLE
A Novel Hand-Held Optical Imager with Real-Time Co-registration Facilities toward Diagnostic Mammography

5a. CONTRACT NUMBER
W81XWH-09-1-0004

5b. GRANT NUMBER
BC083282

5c. PROGRAM ELEMENT NUMBER

6. AUTHOR(S)
Sarah J. Erickson
Email: sarah.erickson@fiu.edu

5d. PROJECT NUMBER

5e. TASK NUMBER

5f. WORK UNIT NUMBER

7. PERFORMING ORGANIZATION NAME(S) AND ADDRESS(ES)
Florida International
University
MARC 430
11200 SW 8th Street
Miami, FL 33199

8. PERFORMING ORGANIZATION REPORT NUMBER

9. SPONSORING / MONITORING AGENCY NAME(S) AND ADDRESS(ES)
U.S. Army Medical Research and Materiel Command
Fort Detrick, Maryland
21702-5012

10. SPONSOR/MONITOR'S ACRONYM(S)

11. SPONSOR/MONITOR'S REPORT NUMBER(S)

12. DISTRIBUTION / AVAILABILITY STATEMENT
Approved for public release; distribution unlimited

13. SUPPLEMENTARY NOTES

14. ABSTRACT

Hand-held based optical imaging devices using near-infrared (NIR) light are currently developed toward clinical translation of the technology. However, none of the NIR devices developed to date have attempted 3D tomography since they are not able to coregister the image to the tissue geometry. The objective for the work described herein is the clinical translation of a hand-held optical imager with automated coregistration facilities toward 3D tomography. Studies were performed *in vivo* with normal human subjects to demonstrate fast (near real-time) 2D fluorescence imaging for target detection prior to 3D tomography. The results showed that 0.23 cm^3 and 0.45 cm^3 fluorescent targets placed behind the breast tissue were detected through ~2.5 cm deep tissue. Parallely, studies were performed on phantoms composed of minced chicken breast and 1% Liposyn solution to demonstrate coregistered imaging *in vitro*. The results showed that the 3D tracking system was able to track the position of the probe in real-time and accurately coregister the image to the geometry of the object. Additionally, deeper targets can be detected upon summation of multiple coregistered images. These results demonstrate the potential of the device to perform 3D tomographic imaging in human subjects via coregistered imaging on complex breast geometries.

15. SUBJECT TERMS
Diffuse optical imaging, near-infrared, breast cancer, hand-held device, fluorescence, coregistration, in-vivo

16. SECURITY CLASSIFICATION OF:			17. LIMITATION OF ABSTRACT	18. NUMBER OF PAGES	19a. NAME OF RESPONSIBLE PERSON
a. REPORT	b. ABSTRACT	c. THIS PAGE			USAMRMC
U	U	U	UU	29	19b. TELEPHONE NUMBER *(include area code)*

Table of Contents

Page

A Novel Hand-Held Optical Imager with real-Time Coregistration Facilities toward Diagnostic Mammography

Annual Report (Year 1, Jan 2009-Dec 2009)

PI: Sarah J. Erickson (seric001@fiu.edu)
Contact Details: Doctoral Student, Department of Biomedical Engineering
College of Engineering and Computing, Florida International University, Miami, FL
Grant No. BC083282
Mentor: Dr. Anuradha Godavarty (godavart@fiu.edu)

INTRODUCTION

Optical imaging using near-infrared (NIR) light is an emerging technique toward non-invasive breast cancer diagnosis. Hand-held based optical imaging devices are currently developed toward clinical translation of the technology.[1] However, the NIR devices developed to date have not attempted three-dimensional (3D) tomography since they are not able to accurately coregister the image to the geometry of the object. ***The overall goal of the research is to implement and test a novel hand-held based optical imager with capabilities of automated coregistration on any tissue curvature for real-time surface imaging and 3D tomographic analysis, on tissue phantoms and in vivo with human subjects.*** The purpose for this research is to translate the device to the clinical setting for breast cancer imaging. The scope of the research involves experimental studies on tissue phantoms and *in vitro*, and *in vivo* studies with normal human subjects prior to clinical studies with breast cancer patients.

BODY

The tasks that were completed in Year-1 of the proposed projects are described herein. The tasks were categorized according to three specific aims as outlined in the statement of work:

Specific Aim# 1:

Demonstrate imaging and 3-D tomography using hand-held probe on different curved tissue phantoms.

Work Completed to Date:

Proposed Task A: *Modify probe design to achieve uniform source intensity.*

The current design of the hand-held device (shown in Figure 1) utilizes a single laser diode source and a custom built collimator package which divides the laser light among six optical fibers attached to the probe face. The limitation of this design is that the output intensity of the laser light is not divided equally among the six fibers. The goal of this task was to modify the

collimator package in order to achieve the desired uniform source intensity distribution. However, during the course of this task, it was found that achieving uniform intensity distribution is difficult using a single laser diode. Hence, a new design was developed to use six laser diodes individually attached to the six optical fibers which can be adjusted individually to the desired intensity. This design is currently carried out in a parallel project by a team of graduate and undergraduate students in our lab and will be implemented with the second generation of the optical imaging system.

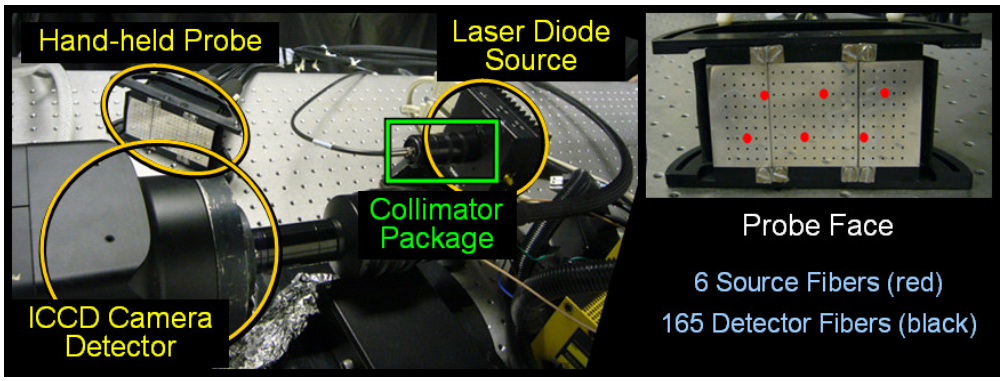

Figure 1. The three major components of the hand-held device (left) are the hand-held probe, the intensified charge-coupled device (ICCD) camera detector, and the laser diode source. The light from the single laser diode source is divided via a collimator package into six source fibers at the probe face (right).

Proposed Task B: *Perform experiments using the hand-held probe in the curved position on curved tissue phantoms.*

Experiments were carried out using the probe in the maximum curved position (45° curvature of each wing) on octagonal phantoms designed to fit the curvature of the probe with full contact. During these studies, it was found that there was interference in the collected signal due to the sharp edges of the octagonal phantom. These studies were discontinued. Further studies focused directly on human breast tissues to demonstrate imaging of curved geometries in the realistic case. *In vivo* studies were performed on normal human subjects to demonstrate the feasibility of using the hand-held device to perform fast 2D imaging toward target detection prior to 3D tomography studies. The device was used to collect images of a fluorescent target with a background of real human breast tissue. Fast imaging was performed in near real time (~5 sec). All human subject studies were approved by the Florida International University Institutional Review Board. Healthy female volunteers age 21 and above were recruited for the studies. A fluorescent target (acrylic sphere filled with 1 μM indocyanine green) was used to simulate a tumor and was placed underneath the flap of the breast tissue (i.e. between breast tissue and chest wall, underneath the tissue). Table 1 gives a summary of the *in vivo* experimental cases performed.

Table 1 Summary of experimental cases performed for *in vivo* fast 2D imaging studies.

Experimental Case #		Number of Targets	Target Depth (cm)	Target Volume (cc)	T:B Contrast Ratio
In vivo with normal human subject	1	1	2.5	0.23	1:0
	2	1	2.5	0.45	1:0
	3	2	2.5	0.23 & 0.45	1:0

Figure 2 shows the results of images (i.e. 2D surface contour plots of fluorescence intensity) collected with the probe in both the flat (Figure 2A) and curved (Figure 2B) position. When the probe was in the flat position, it was placed with gentle compression against the tissue surface to allow full contact with the probe face, whereas in the curved position it was able to contour around the tissue in its natural shape.

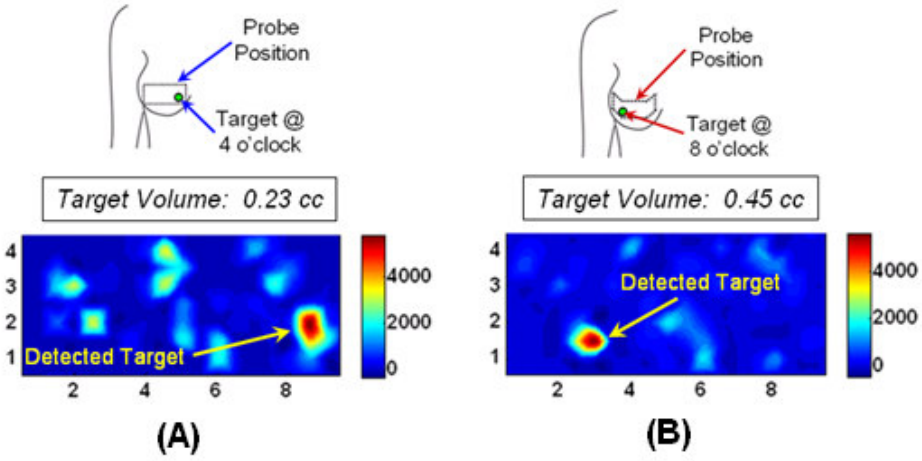

Figure 2. Results for *in vivo* studies with normal human subjects. (A) 0.23 cc target was placed at the 4 o'clock position and imaged with the probe in the flat position. (B) 0.45 cc target was placed at the 8 o'clock position and imaged with the probe in the curved position.

The results show that a fluorescent target was detectable through ~2.5 cm of actual human breast tissue using the probe in both the flat and curved positions. The results for these studies were published in *Translational Oncology*[2] and the article in press is attached in Appendix A.

Specific Aim # 2:

Implement 3-D automated co-registration using acoustic-based tracking system in order to perform real-time in-vivo optical imaging.

Work Completed to Date:

Proposed Task A: *Implement a 3D motion tracking device in order to randomly track the movement of the hand-held probe.*

Coregistered imaging is required in order to perform 3D tomography since the 2D image must be located in the exact position of the hand-held probe on the tissue surface. A 3D tracking system was implemented on the probe in order to perform coregistered imaging using MATLAB/LabView software developed by a master's student in house. Experimental studies using an exogenous fluorescent contrast agent Indocyanine Green (ICG) were performed to demonstrate the feasibility of coregistered imaging using the hand-held probe based optical imager. The contrast agent is placed in a small spherical target and embedded within the phantom to represent a tumor within a tissue background. Successful implementation of the coregistered tracking method would be indicated by the ability to track the actual location of the target as the probe is moved to different positions with respect to the phantom surface. Coregistered imaging was demonstrated in slab tissue phantoms (composed of 1% Liposyn) and the results published in *Review of Scientific Instruments*[3] (article in press is attached in Appendix B). Additional experiments were performed in phantoms composed of minced chicken breast combined with 1% Liposyn to demonstrate coregistered imaging *in vitro*, and the results were published in *Review of Scientific Instruments* (Appendix B).[3] ***The results showed that the 3D tracking system was able to track the position of the probe in real-time and accurately coregister the image to the geometry of the object in tissue phantoms and in vitro.*** During these coregistered imaging studies, it was found that by collecting multiple coregistered images and applying a post-processing summation technique, a target can be detected at greater depths than with a single image alone. A 0.45 cm^3 target was detected at a depth of 3.0 cm in the slab tissue phantom, and a 0.45 cm^3 target was detected at a depth of 2.5 cm in the ***in vitro*** phantom.[3] ***These results show that by summating multiple coregistered images, deeper targets can be detected.*** Ongoing studies are currently performed to determine the deepest and smallest size target that can be detected using this technique.

Proposed Task B: *Adapt and improve 3D reconstruction tools for optical tomography studies.*

This task is part of ongoing research to be completed in subsequent years.

Specific Aim # 3:

Perform feasibility in-vivo studies using diffuse optical imaging on normal subjects to demonstrate real-time co-registered imaging.

Proposed Task A: *Perform in-vivo studies with ~5 normal human subjects at Florida International University.*

This task is part of ongoing research to be completed in subsequent years.

Proposed Task B: *Implement the tracking system to obtain real-time surface images of the human breast tissues using the hand-held optical imager.*

This task is part of ongoing research to be completed in subsequent years.

Training Plan:

Instrumentation and Phantom Studies:

The P.I. trained under a previous doctoral student to learn how to operate the imaging system and carry out experiments using tissue phantoms.

In Vivo Studies

The P.I. received training from Sylvester Cancer Center under Dr. Richard Kiszonas. The training involved observing breast imaging (i.e. x-ray mammography and breast ultrasound) and interacting with doctors and technicians in the clinical setting.

Mentoring

During Year-1 the P.I. mentored two undergraduate students in performing *in vivo* studies, a third undergraduate student in instrumentation, and a master's student in coregistered imaging and instrumentation.

KEY RESEARCH ACCOMPLISHMENTS

- Demonstrated fast 2D imaging using the hand-held device on curved tissue geometries in normal human subjects.
  (Specific Aim #1)
- Detected fluorescent targets *in vivo* within actual human breast tissue.
  (Specific Aim #1)
- Implemented 3D tracking system and demonstrated coregistered imaging using the hand-held device on tissue phantoms and *in vitro*.
  (Specific Aim #2)
- Detected deeper targets by applying multi-scan summation technique using coregistered images.
  (Specific Aim #2

REPORTABLE OUTCOMES

Peer-reviewed Journal Publications

(1) **S.J. Erickson**, J. Ge, A. Sanchez, and A. Godavarty. "Two-dimensional fast surface imaging using a hand-held optical device: in-vitro and in-vivo fluorescence studies," Translational Oncology (in press, 2009).

(2) S. Regalado, **S. J. Erickson**, B. Zhu, J. Ge, and A. Godavarty. "Automated coregistered imaging using a hand-held probe-based optical imager," Review of Scientific Instruments (in press, 2009).

(3) J. Ge, **S.J. Erickson**, and A. Godavarty. "Fluorescence tomographic imaging using a hand-held probe based optical imager: extensive phantom studies," Applied Optics 48(33), 6408-6416 (2009).

National Conference Proceedings (presenter)*

(1) **S.J. Erickson***, J. Ge, and A. Godavarty. "Clinical Translation of a Novel Hand-Held Based Optical Imager: *In Vitro* and *In Vivo* Studies," IFMBE Proceedings 25th Southern Biomedical Engineering Conference 2009, 15 -- 17 May 2009, Miami, Florida, USA; 24: 3-4; A.J. McGoron, C.Z. Li, and W.C. Lin, eds. ISBN: 978-3-642-01696-7 (2009).

(2) J. Ge, **S.J. Erickson***, and A. Godavarty. "Fluorescence Tomographic Imaging Using a Hand-Held Optical Imager: Extensive Phantom Studies," IFMBE Proceedings 25th Southern Biomedical Engineering Conference 2009, 15 -- 17 May 2009, Miami, Florida, USA; 24: 1-2; A.J. McGoron, C.Z. Li, and W.C. Lin, eds. ISBN: 978-3-642-01696-7; 2009.

Abstracts (accepted)

(1) **S.J. Erickson,** S. Martinez, J. DeCerce, L. Caldera, A. Godavarty. "Fast coregistered imaging in vivo using a hand-held optical imager," SPIE Photonics West, San Francisco, CA, Jan. 23-28, paper #7555-25 (2010).

Awards

(1) **Lydia I. Pickup Scholarship**, Society of Women Engineers, 2009

(2) **1st Place Doctoral Student Award**, SBEC 2009 Paper Competition, 25th Southern Biomedical Engineering Conference, Miami, FL

(3) **3rd Place Best Student Poster Award** 2009 NIH-SPIE Workshop, Bethesda, MD

(4) **3rd Place Paper Competition Award**, Engineering Division, 2009 Scholarly Forum, Florida International University

Funding Received

(1) Coulter Early Career Translational Award (to PI's mentor): The initial in-vivo results from the PI's work served as strong preliminary results in the proposal to Coulter Foundation, leading to the funding of a 2-year project for the PI's mentor.

CONCLUSION

The objectives outlined in the statement of work that have been completed to date are Specific Aim #1 and part of Specific Aim #2. The major outcomes from these tasks are: (i) demonstration of fast 2D imaging using the hand-held device on curved tissue geometries and detection of a fluorescent target in actual human breast tissue, (ii) implementation of a 3D tracking system and demonstration of coregistered imaging using the hand-held device on tissue phantoms and *in vitro*, and (iii) detection of deeper targets using summation of multiple coregistered images. The results obtained were published in the peer-reviewed journals *Translational Oncology* and *Review of Scientific Instruments* and presented at the national meetings *SPIE Photonics West* and *Southeastern Biomedical Engineering Conference*.

The results from these tasks demonstrate the ability of the hand-held device to image in human breast tissues which have complex geometries, whereas previous studies used slab phantoms with simple geometries. A fluorescent target was detected *in vivo* through human breast tissue which demonstrates the potential of the device to detect a tumor in the clinical setting. A tracking system was implemented with the hand-held device and coregistered imaging was demonstrated on tissue phantoms and *in vitro*. These results demonstrate the ability of the device to accurately coregister the image to the geometry of the object and hence the potential of the device to perform 3D tomographic imaging in human subjects via coregistered imaging on complex geometries.

REFERENCES

(1) **S.J. Erickson** and A. Godavarty. "Hand-Held Based Near-Infrared Optical Imaging Systems: A Review" Medical Engineering and Physics 31, 495-509 (2009).

(2) **S.J. Erickson**, J. Ge, A. Sanchez, and A. Godavarty. "Two-dimensional fast surface imaging using a hand-held optical device: in-vitro and in-vivo fluorescence studies," Translational Oncology (in press, 2009).

(3) S. Regalado, **S. J. Erickson**, B. Zhu, J. Ge, and A. Godavarty. "Automated coregistered imaging using a hand-held probe-based optical imager," Review of Scientific Instruments (in press, 2009).

APPENDICES

The following appendices are attached:

Appendix A:

S.J. Erickson, J. Ge, A. Sanchez, and A. Godavarty. "Two-dimensional fast surface imaging using a hand-held optical device: in-vitro and in-vivo fluorescence studies," Translational Oncology (in press, 2009).

Appendix B:

S. Regalado, **S. J. Erickson**, B. Zhu, J. Ge, and A. Godavarty. "Automated coregistered imaging using a hand-held probe-based optical imager," Review of Scientific Instruments (in press, 2009).

Translational Oncology
www.transonc.com

Volume X Number Y Month 2009 pp. 1–7 1

Brief Article

Two-dimensional Fast Surface Imaging Using a Handheld Optical Device: *In Vitro* and *In Vivo* Fluorescence Studies[1]

Sarah J. Erickson, Jiajia Ge, Andrea Sanchez and Anuradha Godavarty

Department of Biomedical Engineering, Florida International University, Miami, FL 33174, USA

Abstract

Near-infrared (NIR) optical imaging is a noninvasive and nonionizing modality that is emerging as a diagnostic tool for breast cancer. The handheld optical devices developed to date using the NIR technology are predominantly developed for spectroscopic applications. A novel handheld probe–based optical imaging device has been recently developed toward area imaging and tomography applications. The three-dimensional (3D) tomographic imaging capabilities of the device have been demonstrated from previous fluorescence studies on tissue phantoms. In the current work, fluorescence imaging studies are performed on tissue phantoms, *in vitro*, and *in vivo* tissue models to demonstrate the fast two-dimensional (2D) surface imaging capabilities of this flexible handheld-based optical imaging device, toward clinical breast imaging studies. Preliminary experiments were performed using target(s) of varying volume (0.23 and 0.45 cm^3) and depth (1-2 cm), using indocyanine green as the fluorescence contrast agent in liquid phantom, *in vitro*, and *in vivo* tissue models. The feasibility of fast 2D surface imaging (~5 seconds) over large surface areas of 36 cm^2 was demonstrated from various tissue models. The surface images could differentiate the target(s) from the background, allowing a rough estimate of the target's location before extensive 3D tomographic analysis (future studies).

Translational Oncology (2009) X, 1–7

Introduction

Handheld-based optical imaging devices have been developed for breast imaging to accelerate the clinical translation of the technology toward cancer diagnosis. Several of these handheld devices have been tested *in vivo* on human subjects [1 2 3 4 5, selected publications]. However, they are unable to contour to the curvature of human breast tissue because all these devices used flat-probe faces. The predominant applications to date have been either toward spectroscopic measurement of tissue optical properties or two-dimensional (2D) localization studies of abnormal tissue within the breast. Recently, a handheld optical imaging device has been developed in our Optical Imaging Laboratory [6] toward imaging large tissue surfaces using a flexible probe face that contours to different tissue curvatures. The device is intended to augment current clinical imaging modalities for breast cancer detection and diagnosis. The three-dimensional (3D) tomographic ability of the device has been demonstrated on large tissue phantoms using a fluorescence-enhanced–based imaging technique [7]. Herein, preliminary studies are performed on tissue phantoms, *in vitro*, and *in vivo* tissue models to demonstrate the fast 2D surface imaging capabilities of this flexible handheld-based optical imaging device toward clinical breast imaging studies.

Materials and Methods

Instrumentation

The instrumentation for the handheld optical imaging device consists of a 785-nm, 500-mW laser diode source and an intensified charge-coupled device (ICCD) camera detector (with 550-850 nm bandwidth at the intensifier end) as shown in Figure 1. The source light is launched onto and collected from the tissue surface using a handheld-based probe head (4 × 9-cm^2 imaging area). The handheld probe consists of 6 points of illumination and 165 points of collection (as shown in Figure 2) of optical signals through optical fibers, which connect the probe head to the source and detector. The total

Address all correspondence to: Anuradha Godavarty, Department of Biomedical Engineering, Florida International University, Optical Imaging Laboratory, 10555 W Flagler St, EC 2675, Miami, FL 33174. E-mail: godavart@fiu.edu

[1]The authors thank the Florida Department of Health (08BB-06) and Department of Defense (BC083282) for their funding support.
Received 6 June 2009; Revised 8 September 2009; Accepted 15 September 2009

DOI 10.1593/tlo.09157

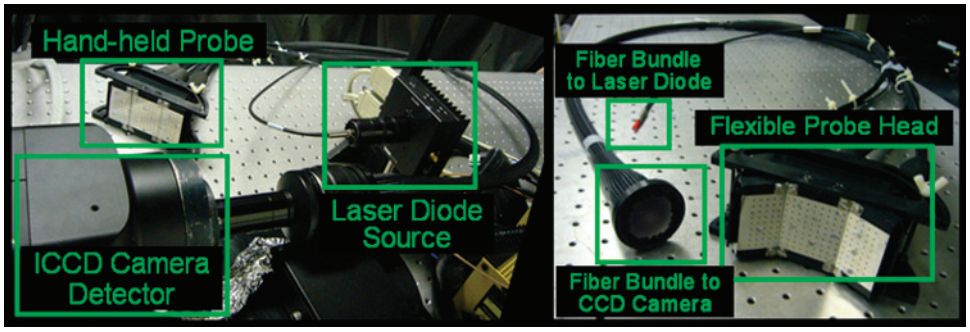

Q3 **Figure 1.** Handheld probe–based optical imaging system showing the handheld probe is fiber-optically coupled to the laser source and ICCD camera (left). The probe face is flexible to contour to different tissue curvatures (right).

laser power incident on the phantom or tissue is <10 mW. The device has a flexible probe head design such that it contours to different tissue curvatures during imaging. Simultaneous illumination and detection from multiple point locations is carried out to reduce the overall imaging time. Additional details of the instrumentation are provided elsewhere [7]. The instrumentation is developed such that it can acquire both continuous wave (CW)–based and frequency-domain–based optical measurements as required. To facilitate 2D imaging in real time, the device was operated in the CW mode for the current study in tissue phantoms, *in vitro*, and *in vivo*.

Data Acquisition and Analysis

Two-dimensional surface imaging was performed, using the handheld device operated in the CW mode, on tissue phantoms, *in vitro*, and *in vivo* tissue models. In all cases, fluorescence-enhanced imaging was performed using an external fluorescing agent indocyanine green (ICG) for improved contrast. Spherical acrylic targets (of different sizes) filled with 1 μM ICG were used to mimic a tumor. The target was placed at different depths from the imaging surface and different target-to-background (T:B) contrast ratios (1:0 and 100:1) were used for different experimental cases. The probe was placed in contact with the phantom or tissue surface as shown in Figure 3, and CW images of the fluorescent intensity were acquired in close to real time (~2 seconds' delay). The raw fluorescence intensity images at the ICCD camera end were acquired in 1 second (0.2-second exposure time × 5 repetitions). These images were postprocessed (~1 second) using in-house developed Matlab codes to acquire the final 2D surface contour plots of fluorescence intensity distribution of the imaged surface. The entire data acquisition and postprocessing were automated such that close to real-time (~2 seconds' delay) imaging is possible. The 2D surface contour plots of fluorescence intensity signal may or may not differentiate the target from the tissue phantom background, based on the target and background optical properties.

During fluorescence optical imaging, the output signal at the tissue surface is a mixture of fluorescence signal and the attenuated incident near-infrared (NIR) (i.e., excitation) signal. This fluorescence signal is filtered from the strong excitation signal (three to four orders of magnitude higher) using appropriate optical (band-pass) filters and imaged by the detector. However, the filters are not capable of 100% rejection of the excitation light, causing an excitation leakage and contamination of the fluorescent signal. Hence, a second level of postprocessing is carried out to subtract a background nonfluorescing image from the final fluorescence image plots for each experimental case to account for the excitation leakage. Initially, optical measurements were acquired before placing the fluorescent target in the phantom, in an attempt to represent the excitation leakage (or background noise). These (background noise) measurements were subtracted from the fluorescence optical measurements obtained from experimental cases that included fluorescent targets to effectively eliminate the signal from the excitation source light. In the clinical setting involving actual diseased tissues (unlike the simulated fluorescent targets in the current study), this could be accomplished by acquiring image(s) of the tissue before and after the contrast agent (e.g., ICG) injection. The nonfluorescent image(s) acquired before ICG injection will in turn be subtracted from the fluorescent images acquired after ICG injection to account for the background noise.

The subtracted 2D fluorescence images are generated rapidly (<5 seconds), making the entire process a fast 2D surface imaging technique. The acquisition of these subtracted fluorescence 2D surface contour plots has greater significance in 2D target localizations as well as in 3D tomographic imaging studies.

Experimental Cases

Tissue phantom studies. Studies were performed using slab tissue phantoms composed of 10 × 10 × 10-cm^3 acrylic cubes filled with 650 ml of 1% Liposyn solution (Liposyn II, 20%; Henry Schein, Melville, NJ) to mimic the optical properties of a typical breast tissue. The fluorescent target was placed at different depths (1.5-2.5 cm) from

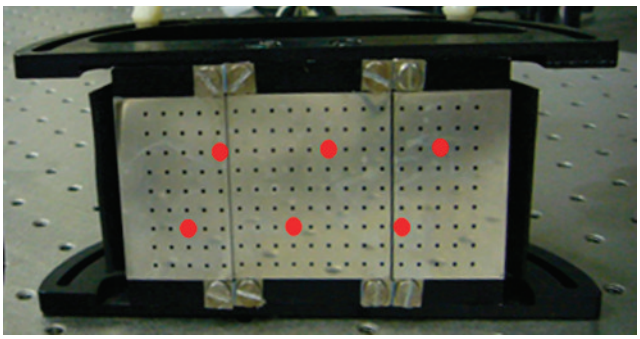

Figure 2. Picture of the handheld probe face showing the source-detector configuration. The large red dots represent the six source fiber locations, and all other small holes are the 165 detector fiber locations.

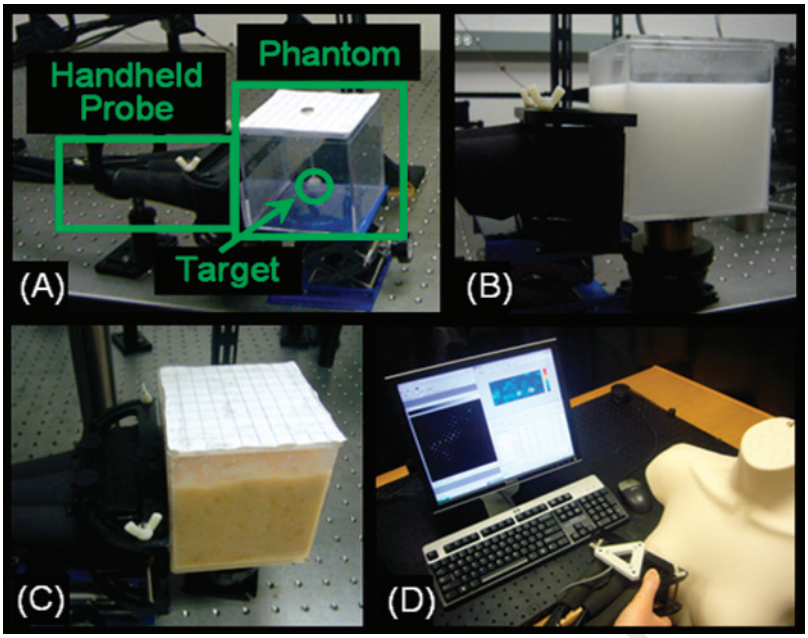

Figure 3. Experimental setup for tissue phantom, *in vitro*, and *in vivo* studies: (A) empty phantom showing target inclusion and placement of probe, (B) tissue slab phantom with 1% Liposyn solution for uniform scattering in the background, (C) *in vitro* slab phantom with heterogeneous scattering in the background, and (D) setup for *in vivo* studies using mannequin (for demonstration only) to represent human subject.

the imaging surface and real-time as well as fast (subtracted) images of fluorescence intensity were acquired. The different experimental cases are summarized in Table 1.

In vitro phantom studies. Before *in vivo* studies with human subjects, experiments were performed using *in vitro* phantoms, which were composed of minced chicken breast combined with 1% Liposyn solution, to introduce a nonuniform scattering background. The *in vitro* mixture of minced chicken breast (480 ml) and 1% Liposyn (260 ml) was placed inside a 10 × 10 × 10-cm^3 acrylic cube. Real-time as well as fast (subtracted) images of fluorescence intensity were acquired under different experimental conditions using either a 0.23-cm^3 or 0.45-cm^3 fluorescent target located at various depths between 1 and 2 cm (Table 1).

In vivo studies. *In vivo* studies were performed on healthy human subjects to demonstrate the feasibility of using the handheld device to collect images of a fluorescent target with a background of real human breast tissue. All human subject studies were approved by the Florida International University Institutional Review Board. Healthy female volunteers aged 21 and older were recruited for the studies. A fluorescent target was used to simulate a tumor (as described in Data Acquisition and Analysis) and was placed underneath the flap of the breast tissue (i.e. between breast tissue and chest wall, underneath the tissue). In the first study, a 0.23-cm^3 sphere with 1 μM ICG was placed under the right breast in the 4-o'clock position. The flat-probe face was placed against the breast tissue with gentle compression, and a real-time fluorescent intensity image was acquired (around the target region). The depth of the target within the tissue was approximately 2.5 cm as measured with a vernier caliper.

A second study was performed using a single target with the probe in the maximum curved position (i.e., 45° curvature of the two side plates of the three-plate–based probe face). The images collected with the probe in the curved position possibly include transilluminated measurements in addition to reflectance-based measurements. This study was performed to demonstrate the feasibility of using the probe

Table 1. Summary of Experimental Cases for Slab Tissue Phantom, *In Vitro*, and *In Vivo* Studies.

Subject Studied	Experiment No.	Number of Targets	Target Depth (cm)	Target Volume (cm^3)	T:B Contrast Ratio
Slab tissue phantom (uniform scattering in background)	1	1	1.5	0.45	1:0
	2	1	2.0	0.45	1:0
	3	1	2.5	0.45	1:0
In vitro phantom (nonuniform scattering in background)	4	1	1.0	0.45	1:0
	5	1	1.5	0.45	1:0
	6	1	2.0	0.45	1:0
	7	1	1.0	0.23	1:0
	8	1	1.5	0.23	1:0
	9	1	2.0	0.23	1:0
In vitro with healthy human subject	10	1	2.5	0.23	1:0
	11	1	2.5	0.45	1:0
	12	2	2.5	0.23 and 0.45	1:0

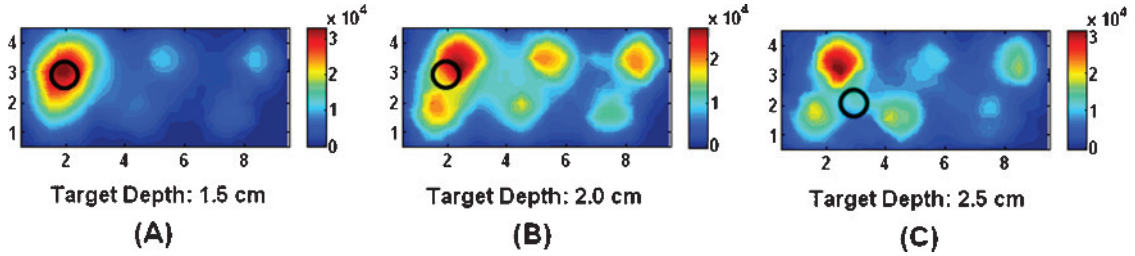

Figure 4. Near real-time images of fluorescence intensity obtained as 2D surface contour plots acquired from slab phantoms (with uniform background scattering). The fluorescent target was placed at different locations and depths: (A) target location (x,y,z) = (2.0, 2.7, 1.5), and (B) target location (x,y,z) = (2.0, 2.7, 2.0), and (C) target location (x,y,z) = (3.0, 2.2, 2.5). The black hollow circle in each subplot is the true target location.

in its curved position, such that it can contour along the tissue and also provide fluorescent images that can aid in target detection. Herein, a 0.45-cm^3 fluorescent target containing 1 μM ICG was placed under the right breast in the 8-o'clock position. A real-time as well as fast (subtracted) image of fluorescence intensity was acquired by applying gentle compression along the tissue curvature.

A third study was performed to demonstrate the feasibility of imaging multiple targets within real human breast tissue. Two targets were placed under the fold of the left breast tissue, with a 0.23-cm^3 target at the 6-o'clock position, and a 0.45-cm^3 target was placed at the 8-o'clock position of the same breast. A real-time as well as fast (subtracted) image of fluorescence intensity was acquired by applying gentle compression on the left breast tissue.

All these preliminary *in vivo* studies used micromolar concentrations of ICG in the tumor-mimicking target(s), similar to the current tissue phantom, *in vitro* phantom studies, and also that used by other researchers [7–9]. The actual *in vivo* studies on breast cancer subjects cannot estimate the concentration of ICG (after injection) at the tumor site, and the researchers typically report the injected quantities of the contrast agent [8,10].

Results

Tissue Phantom Studies

Real-time images using the slab phantom with uniform scattering in the background are shown in Figure 4 as 2D surface contour plots of the fluorescence intensity data with a target placed at different depths (1.5-2.5 cm) from the imaging surface. The nonuniform intensity distribution in Figure 4 is possibly due to the residual excitation leakage around the six source fibers (after the implementation of the subtraction technique). In addition, the input laser source signal is not evenly distributed among the six source fibers, possibly causing a variation or nonuniformity in the output fluorescence intensity distribution.

The images show the feasibility of performing (close to) real-time 2D imaging using the handheld device in tissue phantoms. The actual target location in the images is indicated in the figures by the black open circle in the *x-y* plane for different target depths in the "*z*" direction. The fast 2D image estimates the 2D target location (instantly) in the *x-y* plane. This information can then be further used toward 3D tomography (in the future) to determine the tumor volume, location, and depth [9].

From these plots, it is obvious that the real-time images are capable of differentiating the target from the background when the 0.45-cm^3 target was 1.5 cm deep. At greater tissue depths, the target was not distinctly differentiable because of the strong excitation leakage from the background. On applying the subtraction technique (as described in Data Acquisition and Analysis), the target is clearly differentiable from the background in all the experimental cases (Figure 5). These subtracted images also have potential to obtain 3D target localization through tomographic imaging, as long as the probe's location on the tissue surface is coregistered with respect to the surface fluorescence images.

In Vitro *Phantom Studies*

The results for the *in vitro* phantom experiments are shown in Figures 6 (real-time images) and 7 (fast subtracted images) for different target depths (1-2 cm) under a T:B contrast ratio of 1:0. The true

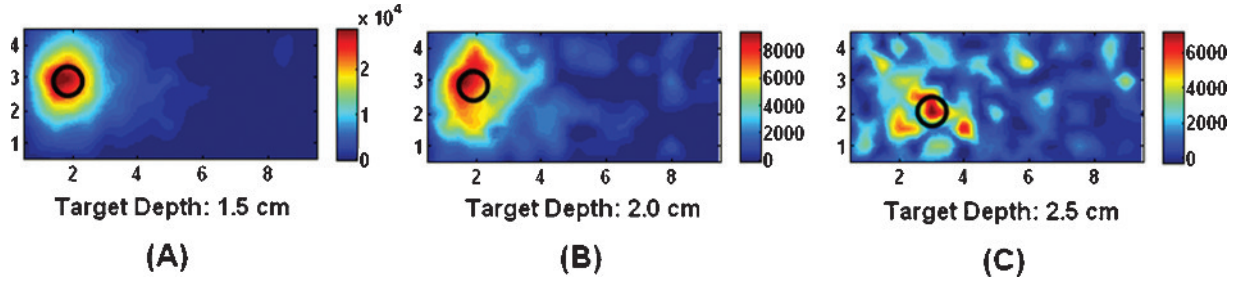

Figure 5. Fast subtracted images of fluorescence intensity obtained as 2D surface contour plots acquired from slab phantoms (with uniform background scattering). The 0.45-cm^3 fluorescent target was placed at different locations and depths: (A) target location (x,y,z) = (2.0, 2.7, 1.5), and (B) target location (x,y,z) = (2.0, 2.7, 2.0), and (C) target location (x,y,z) = (3.0, 2.2, 2.5). The black hollow circle in each subplot is the true target location.

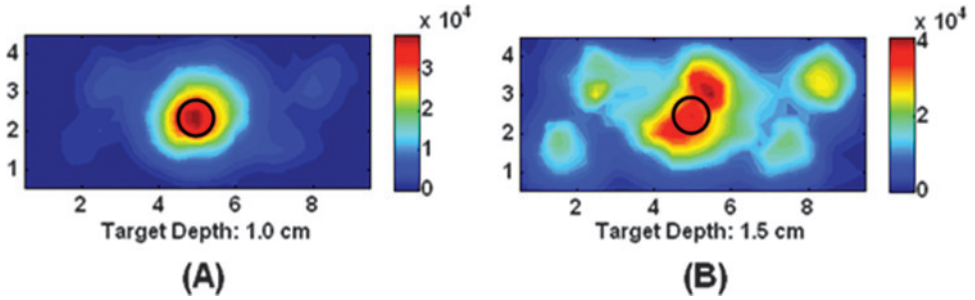

Figure 6. Near real-time images of fluorescence intensity obtained as 2D surface contour plots acquired from *in vitro* slab phantoms (with nonuniform background scattering). The 0.45-cm^3 fluorescent target was located at a depth of (A) 1.0 cm and (B) 1.5 cm from the imaging surface. The black hollow circle in each subplot is the true target location.

target location in the images is given as *x*,*y*,*z* coordinates where "*x*" is the lateral position, "*y*" is the height, and "*z*" is the depth that vary among the images. Owing to heterogeneous scattering of the background phantom, only the subtracted images were capable of clearly differentiating the target from the background for targets deeper than 1.0 cm. These studies show the ability of the handheld device to perform fast 2D surface imaging and target localization within a nonuniform scattering tissue-mimicking background.

In Vivo *Studies*

Figure 8 shows the fast 2D subtracted images of fluorescence intensity obtained *in vivo* (from a healthy human subject using a simulated target) with the probe in the flat position (Figure 8*A*) and in the curved position (Figure 8*B*). These subtracted image results demonstrate the feasibility of fast 2D surface imaging and 2D target localization in a clinical environment. The real-time (nonsubtracted) images of fluorescence intensity were unable to differentiate the target from the heterogeneous background, and hence, only the fast 2D subtracted images are shown in Figure 8.

The 2D subtracted images of fluorescent intensity from multiple simulated targets in a human subject are shown in Figure 9. The 0.23-cm^3 target is detected in the center of the image and the 0.45-cm^3 target is detected toward the left side in the image, which are very close to the true locations of these targets. This study demonstrates the potential to image and localize multiple fluorescent targets (of different sizes) within human breast tissue.

Discussion

The fluorescence imaging studies described here demonstrate for the first time the acquisition of fast 2D surface images (in <5 seconds) of a fluorescent target in uniform tissue phantoms, *in vitro*, and *in vivo* using a handheld-based optical imaging device. The subtracted images have a potential to clearly differentiate target(s) from the background (under various experimental conditions), demonstrating the potential to translate the technology toward on-site breast imaging in a clinical environment. Additional experiments were performed with the target located at greater depths in the tissue phantoms, but the target was not detected at a depth of 2.5 cm. At 2.5 cm deep, the

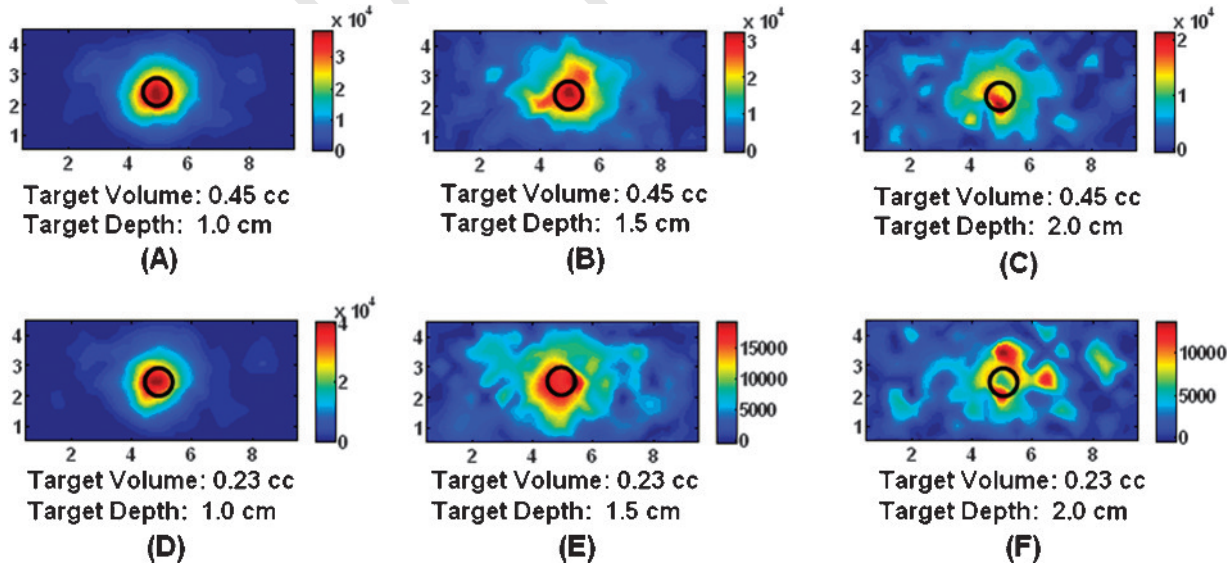

Figure 7. Fast subtracted images of fluorescence intensity obtained as 2D surface contour plots acquired from *in vitro* slab phantoms (with nonuniform background scattering). Images were collected for different target sizes and depths. Images (A) to (C) contain a target size of 0.45 cm^3 at depths of 1.0, 1.5, and 2.0 cm, respectively. Images (D) to (F) contain a target size of 0.23 cm^3 at depths of 1.0, 1.5, and 2.0 cm, respectively. The black hollow circle in each subplot is the true target location.

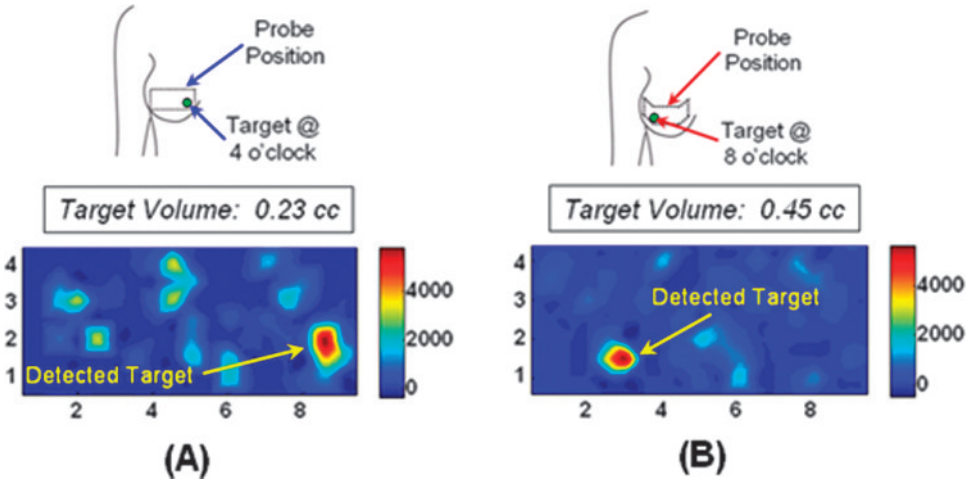

Figure 8. Fast subtracted images of fluorescence intensity obtained as 2D surface contour plots, acquired *in vivo* from a human subject using a spherical fluorescent target, for two experimental cases: (A) the probe was in the flat position and a 0.23-cm^3 target was placed at the 4-o'clock position; and (B) the probe was in the curved position and a 0.45-cm^3 target was placed at the 8-o'clock position. The images acquired using the probe in the curved position are illustrated as projected as a flat 2D image to be consistent with the images presented in case (A) (i.e., using the probe in flat position).

detected signal from the target is close to the noise floor and hence not differentiable from the background. A multilocation scanning approach is currently developed in our laboratory for differentiating deeply located or small-volume targets from homogenous or heterogeneous background [11]. In short, this approach will incorporate the use of coregistered images obtained at multiple locations on the tissue surface, such that the targets can be differentiated from artifacts as well as the background [11]. When comparing Figures 4 and 5, it can be seen that the images from the *in vitro* phantom contain more noise than those from the uniform tissue phantom. This can possibly be attributed to the heterogeneous distribution of scattering properties or shifting of the chicken breast as the target is removed (which can cause a change in the signal distribution when the background image is collected). Experiments were also performed using the *in vitro* phantoms with a T:B contrast ratio of 100:1. However, the noise from the background signal dominated the image, and a target was not detected even after subtracting the excitation background signal. On applying our multilocation scanning approach, the targets were differentiable under imperfect uptake conditions (i.e., T:B = 100:1) [8]. In addition to fast 2D imaging, the handheld device described here has demonstrated 3D tomography of fluorescent targets with tissue phantoms using frequency-domain–based measurements to estimate the 3D location and volume of the target within the tissue [9]. Our ongoing efforts will involve the implementation of fast and automated coregistration facilities to enable precise 2D target localization (instantaneously) as well as 3D tomography studies (*in vitro* as well as *in vivo*).

Conclusions

A handheld-based optical imaging device has been developed in our Optical Imaging Laboratory toward *in vivo* clinical studies on breast

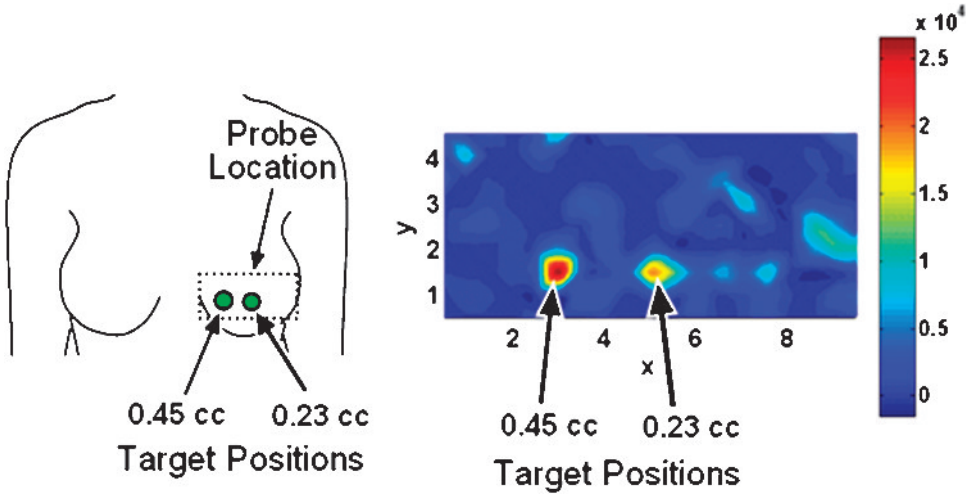

Figure 9. Fast subtracted image of fluorescence intensity obtained as 2D surface contour plot acquired *in vivo* from a human subject using two spherical fluorescent targets (0.23 and 0.45 cm^3).

tissues. The device has been tested extensively in the past on homogeneous slab phantoms (with sample results shown here). The device has been tested for CW-based fluorescence optical imaging *in vitro* as well as *in vivo*. The fluorescence studies demonstrate the ability of the handheld device to perform fast 2D imaging and also detect a fluorescent target within a heterogeneous tissue-mimicking background as well as real human breast tissue (on using subtracted images). Future work will involve fast coregistered imaging of human breast tissue to enable 3D tomography in human subjects using this novel handheld-based optical device.

References

[1] Cerussi AE, Berger AJ, Bevilacqua F, Shah N, Jakubowski D, Butler J, Holcombe RF, and Tromberg BJ (2001). Sources of absorption and scattering contrast for near-infrared optical mammography. *Acad Radiol* **8**, 211–218.

[2] Shah N, Cerussi AE, Jakubowski D, Hsiang D, Butler J, and Tromberg BJ (2004). Spatial variations in optical and physiological properties of healthy breast tissue. *J Biomed Opt* **9** (3), 534–540.

[3] Cerussi A, Shah N, Hsiang D, Durkin A, Butler J, and Tromberg BJ (2006). *In vivo* absorption, scattering, and physiologic properties of 58 malignant breast tumors determined by broadband diffuse optical spectroscopy. *J Biomed Opt* **11** (4), 044005.

[4] Chance B, Nioka S, Zhang J, Conant EF, Hwang E, Briest S, Orel SG, Schnall MD, and Czerniecki BJ (2005). Breast cancer detection based on incremental biochemical and physiological properties of breast cancers: a six-year, two-site study. *Acad Radiol* **12** (8), 925–933.

[5] Zhu Q, Cronin EB, Currier AA, Vine HS, Huang M, Chen NG, and Xu C (2005). Benign *versus* malignant breast masses: optical differentiation with US-guided optical imaging reconstruction. *Radiology* **237**, 57–66.

[6] Jayachandran B, Ge J, Regalado S, and Godavarty A (2007). Design and development of a hand-held optical probe toward fluorescence diagnostic imaging. *J Biomed Opt* **12** (5), 054014.

[7] Godavarty A, Eppstein MJ, Zhang C, Theru S, Thompson AB, Gurfinkel M, and Sevick-Muraca EM (2003). Fluorescence-enhanced optical imaging in large tissue volumes using a gain modulated ICCD camera. *Phys Med Biol* **48** (12), 1701–1720.

[8] Corlu A, Choe R, Durduran T, Rosen MA, Schweiger M, Arridge SR, Schnall MD, and Yodh AG (2007). Three-dimensional *in vivo* fluorescence diffuse optical tomography of breast cancer in humans. *Opt Express* **15** (11), 6696–6716.

[9] Ge J, Zhu B, Regalado S, and Godavarty A (2008). Three-dimensional fluorescence-enhanced optical tomography using a hand-held probe based imaging system. *Med Phys* **35** (7), 3354–3363.

[10] Sevick-Muraca EM, Sharma R, Rasmussen JC, Marshall MV, Wendt JA, Pham HQ, Bonefas E, Houston J, Sampath L, Adams KE, et al. (2008). Imaging of lymph flow in breast cancer patients after microdose administration of a near-infrared fluorophore: feasibility study. *Radiology* **246** (3), 734–741.

[11] Regalado S, Zhu B, Ge J, Erickson SJ, and Godavarty A (submitted 2009). Automated coregistered imaging using a hand-held probe-based optical imager. *Rev Sci Inst*. **Q4**

Automated coregistered imaging using a hand-held probe-based optical imager

Steven Regalado, Sarah J. Erickson, Banghe Zhu, Jiajia Ge, and Anuradha Godavarty[a)]
Department of Biomedical Engineering, Optical Imaging Laboratory, Florida International University, Miami, Florida 33174, USA

(Received 15 June 2009; accepted 9 November 2009; published online xx xx xxxx)

Near-infrared optical imaging holds a promise as a noninvasive technology toward cancer diagnostics and other tissue imaging applications. In recent years, hand-held based imagers are of great interest toward the clinical translation of the technology. However hand-held imagers developed to date are typically designed to obtain surface images and not tomography information due to lack of coregistration facilities. Herein, a recently developed hand-held probe-based optical imager in our Optical Imaging Laboratory has been implemented with novel coregistration facilities toward real-time and tomographic imaging of tissue phantoms. Continuous-wave fluorescence-enhanced optical imaging studies were performed using an intensified charge coupled device camera based imaging system in order to demonstrate the feasibility of automated coregistered imaging of flat phantom surfaces, using a flexible probe that can also contour to curvatures. Three-dimensional fluorescence tomographic reconstructions were also demonstrated using coregistered frequency-domain measurements obtained using the hand-held based optical imager. It was also observed from preliminary studies on cubical phantoms that multiple coregistered scans differentiated deeper targets (~3 cm) from artifacts that were not feasible from a single coregistered scan, demonstrating the possibility of improved target depth detectability in the future. © *2009 American Institute of Physics.* [doi:10.1063/1.3271019]

I. INTRODUCTION

Near-infrared (NIR) optical imaging is a promising noninvasive technology with an indispensable role in breast cancer diagnostics, among many other applications. In recent years, hand-held based optical imaging systems have been developed, as opposed to the other bulky optical imagers available, toward enhancing the clinical translation of the technology.[1–19] The hand-held based NIR imaging systems developed to date are typically designed to obtain surface images and not tomography information, unless they are coupled with another modality toward three-dimensional (3D) tumor localizations.[14–16] The inability to perform tomography is due to limited capabilities to coregister an image with its correct location onto a given tissue geometry. Coregistration is essential in order to accurately determine the probe's position on the 3D tissue geometry during imaging studies, such that the optical measurements can be used toward 3D tomography studies.

Recently, a hand-held based optical probe has been designed and developed in our Optical Imaging Laboratory (OIL), with the following unique features: (i) flexibility to image different tissue curvatures (0°–45°) via a geometrically adaptive probe head, (ii) ability to simultaneously illuminate (at 6 point locations) and collect NIR signals (at 165 point locations) toward rapid data acquisitions, and (iii) portability and comfort from the hand-held design with maximal patient comfort.[3] Preliminary studies demonstrated the feasibility of the hand-held imager to perform 3D tomographic imaging on large slab phantoms (650 cm^3).[4] In these experimental studies, a single probe location with respect to the tissue phantom was predetermined manually and implemented during image reconstructions. However, manual coregistration of the probe onto the tissue phantom may not be feasible at all times, especially during real-time and multiple location scanning on curved and/or nonsymmetric phantoms (e.g., breast tissues). Herein, the hand-held optical imager is improvised and implemented with an innovative coregistration technique which is automated toward real-time coregistered tracking and imaging. Coregistered images were then used toward 3D tomographic imaging of a tissue phantom from a single random scan.

In the upcoming sections, the materials and methods implemented to achieve automated (and fast) coregistered imaging are described. Results from 3D coregistered imaging studies on tissue phantoms follow, in which flat probe face configuration is implemented. Quantitative analyses of these results are then performed to determine the accuracy and precision of the developed coregistration facilities in conjunction with the imager. Additionally, the implications of the coregistration method (in which improved target depth detection can be achieved) are addressed. The feasibility of 3D fluorescence-enhanced tomography studies using coregistered image(s) is also demonstrated.

[a)]Author to whom correspondence should be addressed. Tel.: 305-348-7340. FAX: 305-348-6954. Electronic mail: godavart@fiu.edu.

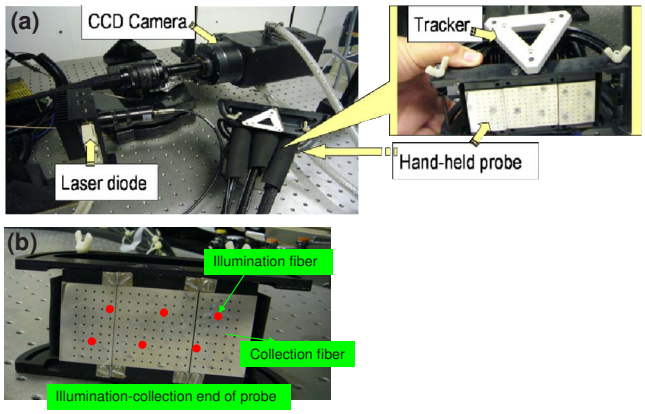

FIG. 1. (Color online) (a) Hand-held probe-based optical imaging system. (b) Illumination-collection fiber layout on the probe head. The solid big red circles are the illumination fiber locations and the remaining black dots are the collection fiber locations.

II. MATERIALS AND METHODS

A. Hand-held probe-based optical imager

The hand-held probe-based optical imaging system (Fig. 1) is developed such that it can acquire images both in the continuous wave (CW) and frequency domain (FD) mode.[3,4] A 5×10 cm^2 probe consisting of multiple (6) sources and (165) detectors is developed and used along with a laser diode source and a gain-modulated intensified charge coupled device (ICCD) camera based detector.

1. Hand-held optical probe

The hand-held probe consisted of 6 simultaneous illuminating and 165 simultaneous collecting points (or fibers), spaced 0.5 cm apart on a 5×10 cm^2 probe head. The appropriate number and distribution of the simultaneous illuminating and collecting optical fibers was chosen such that the total area of fluorescence amplitude was maximized, the regions with very weak or no fluorescence optical signals were minimized, and the signal strength enhanced.[3] The probe head was geometrically adaptive (segmented three-piece design, see Fig. 1) to allow imaging of any given tissue curvature (up to 45°) with good probe-tissue contact and minimal patient discomfort. The major components of the hand-held probe are the probe head constituting the illuminating/collecting optical fibers, a source fiber bundle, and a collection fiber bundle (Romack Inc., Williamsburg, VA). The hand-held optical probe was coupled to the source end (laser diode) and detector end (ICCD camera) via the source and collection fiber bundles, respectively, in order to develop a novel hand-held probe-based optical imager.[4]

2. Imaging system

Laser light (at 785 nm wavelength) is launched onto the tissue phantom using the hand-held probe via a source fiber bundle (consisting of six fibers) coupled to the laser source (on one end) and the probe head (on the other end). The probe collects the optical signals from the tissue surface via the detector fiber bundle (consisting of 165 fibers) and is then imaged by the ICCD camera. Initially, the modulated laser light from the laser diode illuminated the tissue phantom surface via simultaneous illuminating fiber(s) of the hand-held probe (<5 mW at each illumination point). The NIR signal emitted from the tissue phantom surface was acquired by collection fibers of the hand-held probe and imaged using a 16-bit, 1024×1024 pixel CCD camera (PI-SCX, Roper Scientific) that is optically coupled with an image intensifier (FS9910, ITT Night Vision). A focusing lens (50 mm, Nikon Inc.) for image focus and interference filters for excitation light rejection (improved upon using two filters) were coupled to the ICCD camera via a lens assembly.

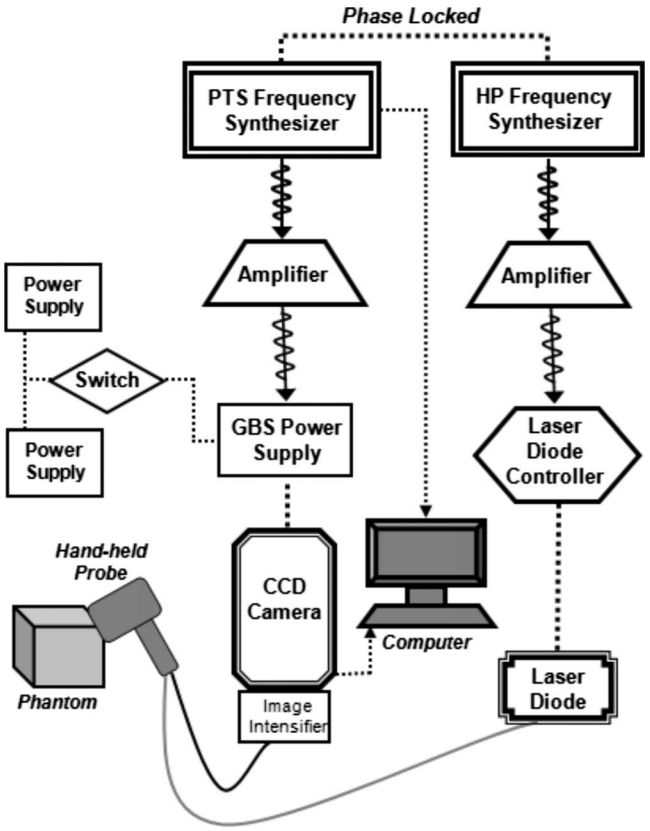

FIG. 2. Schematic of the frequency-domain optical imaging instrumentation, using a flexible hand-held optical probe.

The imaging system was operated in the homodyne mode, meaning that both the source and detector ends are modulated at the same frequency (here 100 MHz) (Fig. 2). The two frequency synthesizers generating the radio frequency (rf) signal at the source and detector end were phase locked. By introducing phase delays varying from 0 to 2π (here 32 delays) between the two frequency synthesizers, steady-state phase-sensitive intensity images were acquired.[4] Fast Fourier Transforms were used to extract the amplitude and phase shift information from the acquired steady-state images. The extracted amplitude and phase shift data were then used toward tomography studies. For all experimental cases, a subtraction-based postprocessing technique was employed for eliminating excitation leakage and all the measurements were referenced in order to account for the instrument effects (details described in Sec. II D).

The hand-held imager is designed to perform simultaneous multiple point illumination and simultaneous multiple

TABLE I. Advantages and disadvantages of different tracking methods.

Tracking method	Advantage	Disadvantage
Manual	• Simple, straightforward • Unlike electromagnetic (EM) trackers, not affected by magnetic fields	Limited to simple/symmetric geometries
Mechanical	• Linear actuators make for easy one-dimensional tracking with high precision • Use of multiple actuators enables multidimensional tracking • Unlike EM trackers, not affected by magnetic fields	Limited mobility
Inertial	• Recent technological advances have facilitated miniaturization • Unlike EM trackers, not affected by magnetic fields	Poor measurement accuracy over time
EM	• Can be obstructed by large objects and still be tracked	Cannot be in the presence of metal objects or even small magnetic fields
Optical	• No direct connection between transmitter and receiver is required • Unlike EM trackers, not affected by magnetic fields	Require a direct line of sight of tracked objects
Acoustic	• Unlike EM trackers, not affected by magnetic fields	Require a direct line of sight of tracked objects

point detection, in order to enhance the total data acquisition rates. In the current studies, the automated coregistered imaging approach and 3D tomographic imaging were demonstrated by operating the imaging system in the CW- and FD-modes, respectively.

B. Automated coregistered imaging approach

Coregistered imaging is the process of lining up at least two images (planar or volumetric) within the same coordinate space. Two types of coregistration techniques that exist include intermodality and intramodality. Intermodality coregistration combines images of different modalities (e.g., CT/MRI, SPECT/MRI, optical/MRI, etc.),[20–22] whereas intramodality coregistration combines images from the same modality (e.g., 3D ultrasound imaging).[23,24] Researchers performing intermodality or intramodality based coregistration employ tracking systems (i.e., position sensors and/or internal/external fiducial markers) for 3D image coregistration and reconstruction in the field of biomedical imaging (a few example citations listed).[25–38]

In the current work, an intramodality coregistration method similar to 3D ultrasound imaging is developed, such that coregistered 3D surface images from two-dimensional (2D) surface data can be obtained. These 3D surface images will in turn be used toward 3D tomographic analysis (as described in Sec. II E). In order to perform coregistered imaging, tracking the imaging probe's (or device's) position and orientation with respect to the tissue/phantom surface being imaged is essential. This tracked 3D positional information is then used to accurately position the acquired optical images onto the tissue geometry. There are several different tracking methods (e.g., manual, mechanical, inertial, electromagnetic, optical, and acoustic) that enable coregistration to be performed by allowing the position and orientation of an object to be known (see Table I for their advantages and disadvantages). For our optical imaging study using the hand-held optical probe, an acoustic tracking method is employed for the following reasons: (i) there is no interference between optical signals from the optical imager and ultrasonic signals from the acoustic tracker and it is (ii) impervious to metallic objects and magnetic fields (which encompass the environment surrounding the optical imaging system) as observed in electromagnetic trackers.

A 3D acoustic-based tracker from Logitech Inc. (Fremont, CA) was employed along with the hand-held probe-based imaging system. The tracking system (or tracker) consists of a transmitter (installed ~2 ft above the hand-held probe and in a direct line of sight with the same), receiver (attached to hand-held probe), and a processing unit. The receiver is lightweight (<15 g) and portable, which has a minimal impact on the probe's inherent mobility; and the transmitter utilizes ultrasound frequencies (23 kHz), which will not interfere with the optical imaging system. The tracking system can determine the 3D location of the probe (or receiver) with respect to the transmitter in real-time within a 5 ft radius and a 100° spherical cone (Fig. 1). The related tracking software (processing unit) was interfaced to a computer via MATLAB such that a tracked object's location is obtained with six degrees of freedom (x, y, z, pitch, yaw, and roll), determining both the object's position and orientation. Coregistered imaging of tissue/phantoms is implemented as a three-stage process (see Fig. 3).

Stage 1. The first stage (probe tracking) tracks the hand-held probe's location with respect to a discretized phantom mesh via the determination of the spatial 3D probe location (steps 1–4 in Fig. 3). The ultrasound-based motion tracker provides six degrees positional information of a single point on the probe, in real-time (step 1 of Fig. 3). The software used to acquire data from the tracker was developed in the MATLAB environment. Here, a 16×1 vector of binary data in 16 byte format was obtained from the tracker when prompted via a direct RS-232 connection to the host computer. These binary data were further concatenated into a single string and converted to decimal format by applying the "bin2dec()" MATLAB function. The resulting set of decimal values correspond to the real time x, y, z, pitch, yaw, and roll of the receiver The MATLAB code was further implemented into a LABVIEW program (developed in-house) in order to automate the process of data acquisition such that as the tracker changes location, the coordinates and orientation change ac-

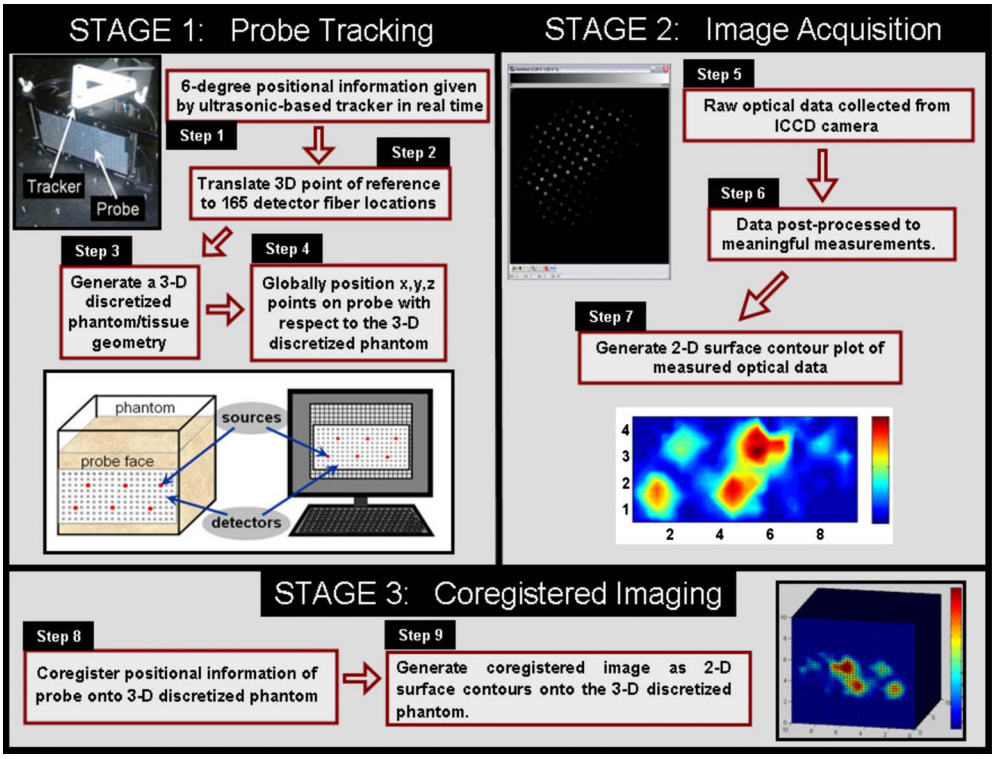

FIG. 3. (Color online) Flowchart of the coregistered imaging process, implemented as automated coregistration software during optical imaging studies.

cordingly, with minimal lag in real time. Initially, the location data of a single reference point on the probe (here the left bottom corner detector of the probe is chosen) is acquired in binary format from the processing unit (of motion tracker) and converted to decimal format using the developed MATLAB code.

Tracking a single point in 3D space is further translated to tracking all the source and detector points (spaced 0.5 cm apart) on the flat probe head (step 2 of Fig. 3). The probe head is built as three-piece plates to allow it to flex along the interfaces of the plates, in order to image tissue curvatures. When the probe head had to be used in its flex (or curved) position, the source and detector locations can be determined from the angle of curvature of the two outer plates. The angle of curvature is determined independently for each outer plate using an angle indicator affixed to the probe. Apart from tracking the source-detector points of the probe head, a 3D discretized phantom or tissue geometry is simulated (step 3 of Fig. 3).

The phantom mesh is a set of discretized data representing the phantom volume, which can be acquired using meshing software (GAMBIT, ANSYS Inc., Canonsburg, PA) or generated within the MATLAB programming environment. For experimental studies, cubical phantom meshes of appropriate volumes were generated in GAMBIT and utilized for coregistration studies. For complex geometries (e.g., *in vivo* cases), a 3D laser scanner may be utilized in order to obtain a simulated 3D phantom/tissue geometry, which can in turn be discretized using a meshing software.

The tracked source-detector points are globally positioned with respect to the 3D discretized phantom (step 4 of Fig. 3) and not yet coregistered. The overall probe tracking is accomplished by utilizing MATLAB/LABVIEW code developed in-house for the acoustic tracker. For a preuploaded discretized phantom mesh onto the coregistration software, the average time to acquire probe tracking for each new probe location is almost in real time (<1 s).

Stage 2. The second stage (image acquisition) involves acquisition of raw optical signals (i.e., steady-state intensity signals) using the hand-held optical imager (step 5 of Fig. 3). These data are postprocessed, using in-house developed MATLAB codes, in order to obtain meaningful optical measurements (i.e., amplitude and phase-shift for FD-based measurements and intensity for CW-based measurements) at their respective point locations on the imaged plane (step 6 of Fig. 3). For each change in location of the probe, a 2D surface image (as contour plot) of optical signals (generated in MATLAB) is generated from the acquired (FD or CW) optical measurements (step 7 of Fig. 3).[4] The images can be from fluorescence-enhanced or nonfluorescence (diffuse) optical imaging studies. The location of each image is simultaneously tracked as described in stage 1, such that a coregistered image could be generated in the subsequent stage. The average time to acquire fluorescence optical measurements and display the data as 2D surface images (contour plots) is ~ 2 s (i.e., 0.2 s exposure time for each of the five repeated measurements, and ~ 1 s for data postprocessing to obtain 2D surface contour plots).

Stage 3. The third stage displays a coregistered image via tracking/coregistration interfacing software developed in MATLAB/LABVIEW (developed in-house). The 2D surface contour plot of optical measurements is coregistered onto the 3D discretized phantom at the probe location using the posi-

tional information of the entire probe head (i.e., all source and detector point locations) during each scan. Coregistration is achieved by determining every source-detector's positional information onto the appropriate x-y-z coordinates of the 3D discretized phantom (step 8 of Fig. 3). This is followed by correlating the obtained fluorescence measurements with respect to the coregistered positional information on the phantom, which represents the actual imaged area on the 3D phantom (step 9 of Fig. 3). The average time for obtaining a coregistered image for a $10\times10\times10$ cm^3 cubical phantom (simulated as a 3D discretized volume mesh) was ~25 s. When only a 3D surface mesh was employed (for a different study), the average time to obtain a coregistered image dropped significantly (~25% of the above time).

The coregistered imaging process is automated for rapid data acquisitions, via the integration of image acquisition software into the tracking/coregistration software. Here automation is defined by allowing the entire data acquisition of coregistered images to be carried out with least operator involvement, such that the displayed optical contour plots are in near real time (with a few seconds delay).

The main features of the developed coregistration software are its ability to (i) upload any set of face and vertex data corresponding to a 3D phantom mesh, (ii) adjust the on-screen position/orientation of a phantom mesh to match its real-time location, (iii) employ simulated or real-time images during coregistration, (iv) autonormalize the contour maps of the acquired images from different locations, with respect to the maximum value of the optical signal (here, optical intensity), (v) retain/erase an image from a previous scan(s), (vi) acquire and display real-time probe location/orientation, (vii) adjust the on-screen angle of the probe's outer plates to match its real-time angles, and (viii) save all displayed information into a single MATLAB file for postprocessing and analysis. The current version of the coregistration software is designed to work with phantoms with known position/orientation and not moving phantoms that need to be tracked, since no tracker is placed on the phantom as with the hand-held probe. In the future, this can be remedied by adding tracking abilities to the phantom (or subject) being imaged, thereby allowing location and orientation of the phantom/tissue to be automatically known and updated in real time.

C. Experimental Studies

Fluorescence-enhanced experimental imaging studies were performed to demonstrate the feasibility of the automated (and fast) coregistered imaging using a hand-held probe-based optical imager. Exogenous fluorescence contrast agent [indocyanine green (ICG)] was used to enhance the optical absorption contrast in tumorlike target(s) to simulate a clinical environment, wherein real-time coregistered optical imaging will be performed.

Successful implementation of the coregistered tracking method would be indicated by the ability to track the actual location of the target even upon moving the probe's location with respect to the phantom surface. Initially, cubical phantoms were chosen to demonstrate one-dimensional, 2D, and 3D coregistered imaging, since the cubical geometry is simple and the probe face can be used in the flat position (i.e., angle of curvature, $\theta=0°$). Herein, only the 3D automated coregistered imaging results are presented for the experimental case employing the probe in its flat position (for cubical phantoms). The effectiveness of automating the fast coregistration method was assessed by evaluating the accuracy and precision of the target location. The accuracy of the coregistration method is determined by calculating the percentage error between the true target location and the experimental target location (i.e., the highest detected intensity corresponding to the centroid of the target) for all scans on each phantom face. The precision of the coregistration method is determined by calculating the standard deviation of the experimental target location for each new scan (which is an average of five repeated images) obtained at varying probe locations.

D. 3D coregistration studies

1. Coregistration studies using a flat probe on cubical phantoms

Cubical phantom studies were performed (using a $10\times10\times10$ cm^3 phantom) in order to evaluate the ability to track a target's location in three dimensions (about an entire phantom volume) while the probe face was in the flat position. The phantom was filled with 850 ml 1% liposyn solution and a 0.45 cm^3 spherical target (filled with 1% liposyn and 1 μM ICG) was submerged 1.5 cm deep from both the x-z and y-z planes of the phantom (centroid location is [1.5, 1.5, 2.8] cm).

The probe was placed flat on the surface of a single face of the cubical phantom and CW-based fluorescence intensity measurements were acquired on the same face at six different locations moving in the vertical "z" direction ([x,y,z] =[0,0,0; 0,0,0.5; 0,0,1.0; 0,0,1.5; 0,0,2.0; 0,0,2.5] cm). Prior to coregistering, the fluorescence intensity data were postprocessed to remove the background noise arising from excitation leakage.[4] This was accomplished by subtracting the intensity plots of a nonfluorescing homogeneous phantom (at the same probe location) from the fluorescence intensity data acquired for the actual experimental case [here, containing fluorescence target(s)]. The final subtracted fluorescence intensity data obtained at all probe locations were normalized with respect to the maximum detected intensity up to that scan, such that all the 2D surface contour plots were on the same scale.

The subtracted and normalized images were coregistered fast (in near real time) onto a 3D discretized phantom surface mesh for each of the six measurements using the developed coregistration software. After each set of measurements was completed on a single face of the phantom, the phantom was rotated 90° in a counter-clockwise direction and another set of measurements (now on a second face) was acquired at a similar location as the first face, with 0.5 cm increments in the probe location along the z-axis. This process was repeated such that four measurement sets resulted from the four faces of the cubical phantom. The fluorescence intensity data were plotted as 2D surface contour plots, which were coregistered directly onto a 3D discretized phantom mesh

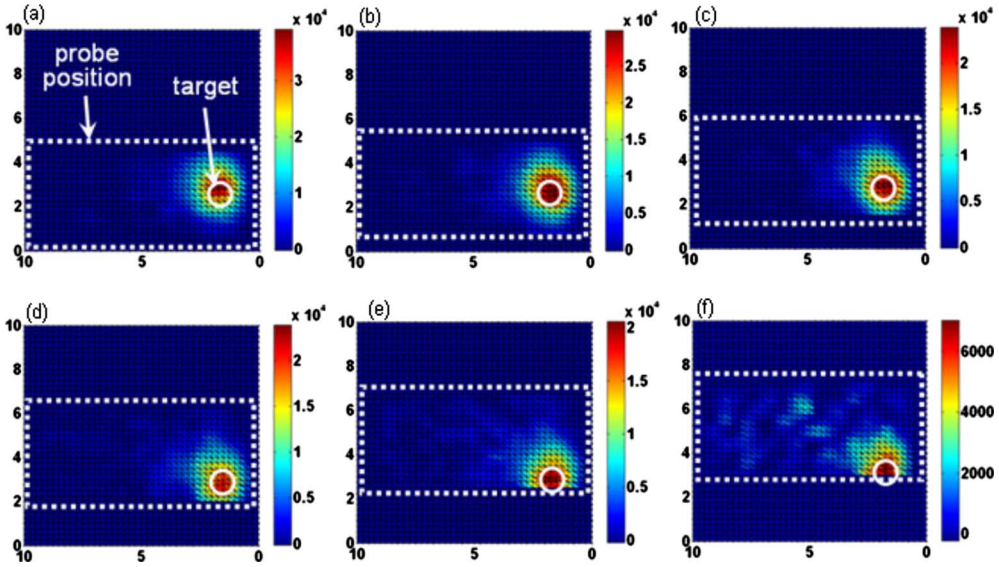

FIG. 4. (Color online) Coregistered surface contour images of fluorescence intensity (subtracted and normalized) obtained from face 1 of a $10\times10\times10$ cm^3 cubical phantom containing a 0.45 cm^3 target located at [1.5, 1.5, 2.8] cm. The white dotted line corresponds to the hand-held probe location on face 1 of the cubical phantom and the white circle corresponds to the true target location in 2D. The probe was moved along the height of the phantom, with its location varying in the increments of 0.5 cm, starting from $z=0$ cm up to 2.5 cm [(a)–(f)].

(generated in GAMBIT and uploaded into MATLAB). In the cubical phantom studies, the phantom was rotated instead of the hand-held probe in order to acquire images from all faces, since the tension in the fiber bundle did not allow the probe's rotation by 90° such that all sides of the phantom are imaged. Instead, the position/orientation of the symmetric phantom was manually acquired and inputted into the coregistration software for the cubical phantom studies.

E. Tomography studies using coregistered measurements

The advantage of implementing a tracking system is the ability to use the obtained fast coregistered measurements toward 3D tomographic studies using a hand-held based optical imager. Frequency-domain based fluorescence measurements (in terms of ac and phase shift) were obtained at a single location of the probe on the phantom and the measurements were coregistered using the above described technique (Sec. II B). A single 0.45 cm^3 fluorescent target filled with 1% liposyn and 1 μM ICG was located at [18.5,14.6, 6.5] cm in a $20\times20\times20$ cm^3 phantom filled with 6000 cm^3 of 1% liposyn solution (with fluorescence optical contrast ratio of 1:0 and at 1.5 cm deep from $x=20$ cm plane). 3D image reconstructions were then performed using the approximate extended Kalman filter (AEKF) based inverse algorithm (see Appendix), which recursively minimizes the variance of parameter error (i.e., error in fluorescence absorption coefficient μ_{axf} for this study) given the estimation of measurement error covariance R, model error covariance Q, and parameter error covariance P. The model error covariance Q was empirically chosen to be equal to 1/4 of the measurement error covariance R, which was estimated from the variances of the means of five repeated experimental measurements[4,39] at each probe location.

Reconstructions were assumed to have converged when the root mean square output error was less than 1%, or the total number of iterations exceeded 50. The absorption coefficient of the fluorophores (μ_{axf}) was the reconstruction parameter, with an initial of $\mu_{axf}=0.003$ cm^{-1}, as assumed for the entire phantom. The reconstructed 3D target centroid, volume and fluorescence absorption coefficient was quantitatively estimated from introducing a cutoff value in the reconstructed μ_{axf} (as the first break point in the histogram of the fluorescence absorption coefficient) in order to differentiate the possible target(s) from the background. Further details of 3D tomography studies performed using the hand-held optical imager can be found elsewhere.[4]

F. Coregistered Imaging toward Improved target depth detection

In this study, CW-based fluorescence imaging studies were performed on a cubical phantom, containing a single fluorescing target (with 1% liposyn and 1 μM ICG) under perfect uptake conditions (i.e., no fluorescence in the background). The target was located 3 cm deep from the phantom face 3 and its centroid location was [3.0, 2.5, 2.8] cm. The coregistered images acquired from multiple locations on each cubical phantom surface (as described in the above sections) were superimposed and summated in order to obtain a 3D coregistered image of the entire cubical phantom. When a summation of fluorescence intensity is performed, trends in intensity patterns for each individual scan that would otherwise appear as random noise may possibly add up to generate an image where the highest intensity corresponds to the sum of weak signals (associated with the true target location). These weak signals from the target location may otherwise not be detectable or differentiable from background noise (or artifacts) when obtained from an individual (or single) scan. The effectiveness of using the summated fluorescence intensity data from multiple scans over the fluorescence intensity obtained from a single scan toward improved

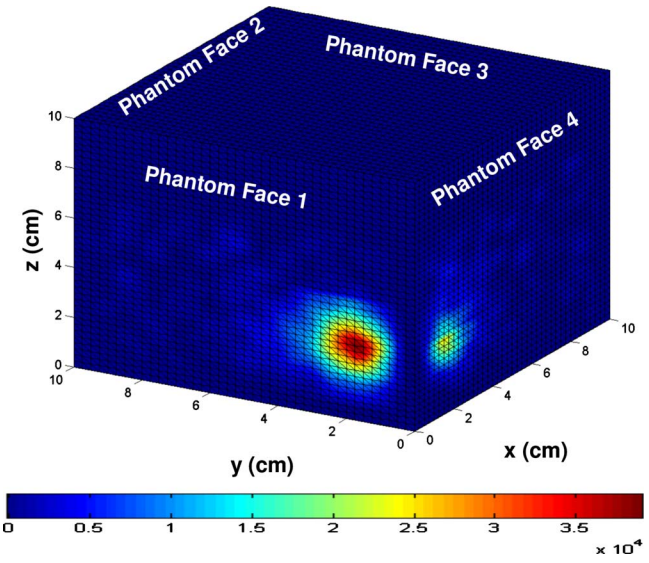

FIG. 5. (Color online) (Enhanced online) The coregistered images (as 2D surface contour plots of subtracted and normalized fluorescence intensity data) of the $10\times10\times10$ cm^3 cubical phantom from multiple scans (along the z-axis) performed on the four faces of the phantom (as shown). The phantom contained a 0.45 cm^3 target at 1:0 fluorescence and optical contrast at [1.5, 1.5, 2.8] cm. Individual coregistered images from each face (as shown for face 1 in Fig. 4) were combined to generate the current 3D plot. The figure also represents single frame excerpts from real-time coregistered imaging of the cubical phantom, with images retained from previous scans. (media 1.09 MB, enhanced online).

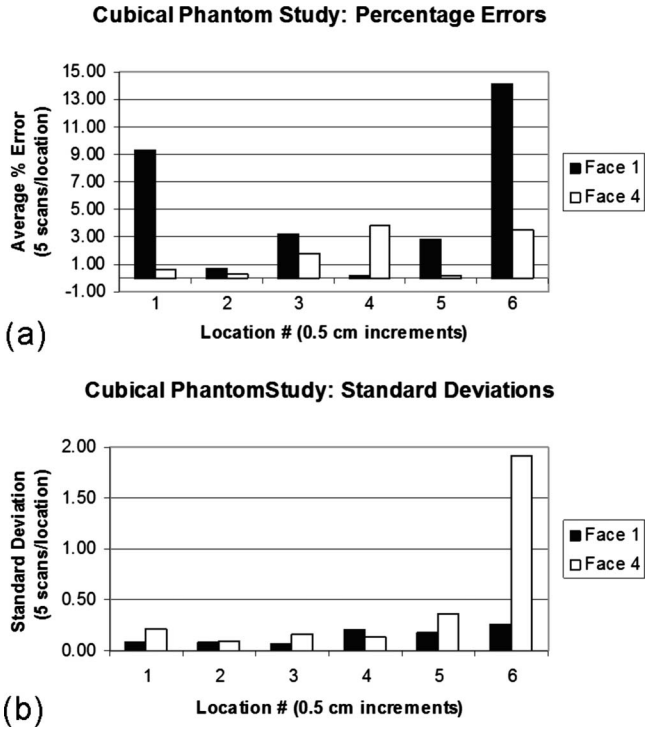

FIG. 6. (a) The percentage error between the true target location and experimental target location for scans 1–6 is shown for phantom faces 1 and 4. The large degree of variability between scans can be attributed to the untracked changes in phantom position and orientation. (b) The standard deviation of five repeated images for each scanned location shown for phantom faces 1 and 4. The large degree of variability between scans can be attributed to instrument error from the optical imaging system due to probe movement against the phantom surface during the period in which the five repeated images were being acquired.

target depth detection is assessed from 2D surface contour plots.

III. RESULTS AND DISCUSSION

A. 3D coregistration studies using the flat probe on cubical phantoms

Figure 4 shows all six coregistered 2D surface contour images obtained from face 1 of the $10\times10\times10$ cm^3 cubical phantom. Figure 5 shows fused coregistered 2D surface contour images obtained on each face of the cubical phantom. A multimedia file is also provided in order to demonstrate automated (fast) imaging capabilities of the imaging system. In the multimedia file, the previous scans are retained as new scans are performed at different faces and locations of the probe with respect to the cubical phantom. The target was located 1.5 cm deep with respect to phantom faces 1 and 4, and was detectable from both these faces and not faces 2 and 3, since it was very deep >8 cm with respect to these faces.

From Figs. 4 and 5, it can be seen that the target was detected closer to the true location, although there was a high degree of variability in target detectability between scans. Evaluation of the automation process was determined by performing a percentage error analysis (which denotes accuracy of the coregistration method) between the true and experimental target locations. The experimental target location was determined by locating the point of highest detected intensity (corresponding to the center of the spherical target) for each of the six scans taken on phantom faces 1 and 4. Figure 6(a) shows a graph of the percentage errors for scans 1–6 on phantom faces 1 and 4. It can be seen from these bar plots [Fig. 6(a)] that the percentage errors vary between scans for both faces. The high degree of variability between scans indicates the occurrence of misaligned coregistrations due to the manual (and possibly inaccurate) tracking of the phantom's position/orientation as it was rotated and held between multiple scans.

In the future, a second motion tracking device is installed onto the phantom geometry, in order to synchronously track both the phantom (or tissue geometry) and the handheld optical probe during imaging studies. This will improve the accuracy of coregistered probe location, which in turn can impact the precision of target localization and tomographic analysis. From a clinical perspective, the inherent motion during breast imaging can be recorded and accounted for, by placing this second motion tracker at a chosen point of reference on the participating subject.

When an individual scan is acquired for one phantom face, the final image is an average of five repeated images taken from the same phantom face in ~1 s. The standard deviation (which denotes precision of the coregistration method) of the highest detected intensity between repeated images is an indicator of the extent to which misaligned coregistrations may have occurred due to instrument errors from the optical imaging system or movement of the probe while it was being held. Figure 6(b) provides a bar plot of the standard deviation for each of the six scanned locations on phantom faces 1 and 4. It can be seen from Fig. 6(b) that there is variability in the standard deviation between re-

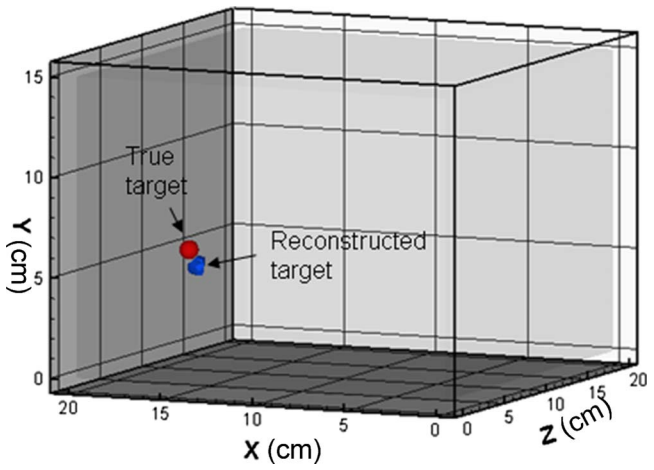

FIG. 7. (Color online) A 3D isosurface plot of the reconstructed tissue phantom showing the reconstructed and the true target location, for an experimental case with 1:0 fluorescence optical contrast of a single 0.45 cm^3 target located 1.5 cm deep (from the x=20 cm plane).

peated images, which indicates that either the probe's position/orientation jitters in the few seconds between the five repetitions, or that there are instrument errors.

B. Tomographic imaging using coregistered measurements

As previously mentioned, coregistered imaging can greatly facilitate tomography by allowing the location of an image to be known with respect to the tissue surface. A single target was reconstructed when inversions were performed using coregistered FD-based fluorescence measurements obtained from a single scan. The reconstructed target's centroid location ([19.6, 13.6, 6.0] cm) was close to its true location of [18.5, 14.6, 6.5] cm as shown from the 3D isosurface plot in Fig. 7 and also quantitative analysis. Since only reflectance-based measurements were used, the target depth recovery (0.4 cm from reconstructions, when the true depth was 1.5 cm) was closer to the surface as observed from our and other researchers' prior studies.[4,19] The y-z (2D) localization of the reconstructed target was slightly off from the true location (1.12 cm), and this could be from experimental error during target placement, since only a single target was reconstructed without any artifacts. Currently, alternate imaging approaches and reconstruction techniques are developed in the laboratory to improve the accuracy in target depth recovery during tomography studies.

From these preliminary studies, feasibility of 3D tomographic imaging using coregistered measurements from a hand-held based optical imager has been demonstrated. In a recent study, 3D tomographic imaging using the same hand-held based optical imager, but manually coregistered fluorescence measurements, has been demonstrated under various experimental conditions,[4] and hence only one experimental case is described here as an example. Reproducibility tomography studies are currently carried out using the automatically coregistered imaging system.

C. Coregistered imaging toward improved target depth detection

Figure 8 shows individual coregistered 2D contour images from six different locations of the cubical phantom face that is closest to the target (located 3 cm deep from this y-z face). It can be seen from these images that in single coregistered scans, a 3 cm deep target is not clearly differentiable from the background. However, when the summed coregistered data are presented as 2D contour images (see Fig. 9), the signal strength at the target location was relatively stronger making the target differentiable from the background. This is possibly because the background noise (or artifacts) does not consistently appear in every scan obtained from varying heights of the same phantom face, but the target does. However, the target being located deeper (3 cm) may have a weaker signal and is not differentiable from the background noise from a single scan. Upon summing the coreg-

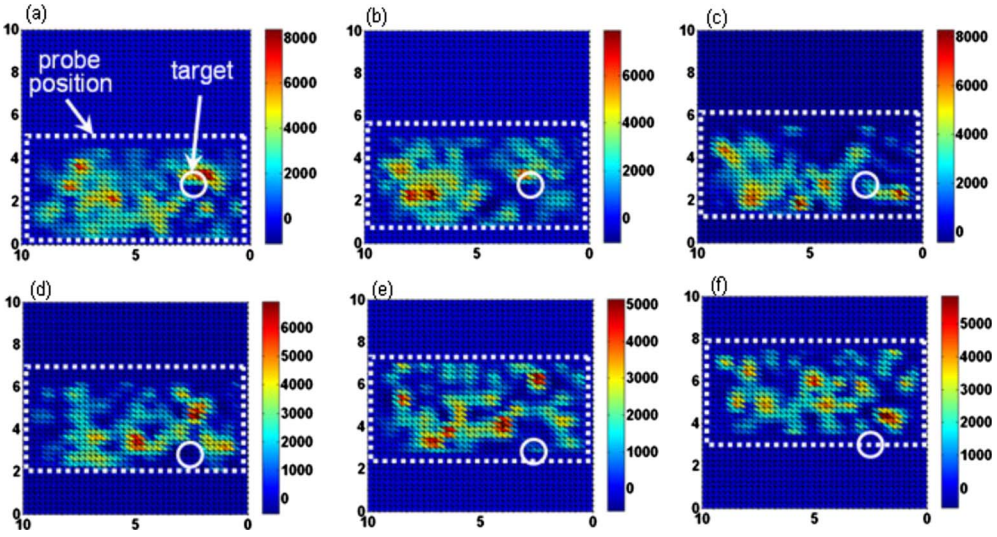

FIG. 8. (Color online) Coregistered surface contour images of fluorescence intensity (subtracted and normalized) obtained from a $10\times10\times10$ cm^3 cubical phantom containing a 0.45 cm^3 target located 3 cm deep at [3, 2.5, 2.8] cm. The white dotted line corresponds to the hand-held probe location on the imaging face of the cubical phantom and the white circle corresponds to the true target location in 2D. The probe was moved along the height of the phantom, with its location varying in the increments of 0.5 cm, starting from x=0 cm up to 2.5 cm [(a–(f)].

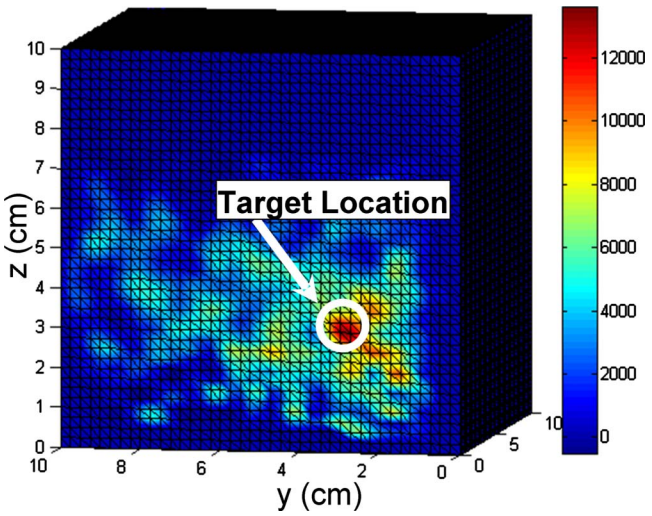

FIG. 9. (Color online) Summated coregistered data shown as 2D surface contour plot of fluorescence intensity obtained from the surface of a 10 $\times 10 \times 10$ cm^3 cubical phantom containing a 0.45 cm target located 3 cm deep. Six coregistered images (shown in Fig. 8) were summated in this case. The white circle is the true target location in 2D.

istered intensity data from multiple scans, the overall intensity at the target location increases significantly with respect to the background random noisy data. Hence, by performing a summation of real-time coregistered data for experimental cases with deeper targets, the ability to detect and differentiate these targets from background noise is improved as demonstrated from these preliminary feasibility studies. The rough estimate of target location can in turn be used as *a priori* information during 3D tomography studies, possibly improving the target depth recovery, especially when fluorescence measurements are obtained from multiple locations and faces of the phantom.

IV. CONCLUSIONS

An innovative coregistration technique has been developed, first of its kind, and implemented onto a hand-held probe-based optical imager such that surface coregistered measurements are obtained toward improved target detection and 3D tomography studies. Continuous-wave and frequency-domain based experimental studies were performed on cubical phantoms to demonstrate the feasibility of 2D automated coregistered imaging and 3D tomographic imaging, respectively. The coregistered optical measurements from multiple scans will be implemented in our image reconstruction algorithms in order to obtain 3D tomographic images of the tissue phantom or *in vivo* tissue. Although all the current experimental studies were fluorescence based, automated (and fast), coregistered and tomographic imaging is also feasible for nonfluorescence diffuse optical imaging.

Since the probe is capable of curving up to 45° on each side, *in vivo* studies on breast tissues are feasible. In the future, (near) real-time *in vivo* optical imaging studies will be performed using the novel hand-held imager, in order to assess the ability to coregister the hand held on actual tissue curvatures. 3D laser scanning devices will be used, such that 3D (discretized) surface maps of the breast tissue are generated. These 3D surface maps will be uploaded on the MATLAB/LABVIEW in-house developed software toward acquiring coregistered images onto the (breast) tissue being imaged. Some of the challenges in the clinical translation of this hand-held imager include: (i) optical measurements can be easily contaminated by motion artifacts caused by patient/operator, (ii) the relative motion of the probe and soft tissue during contact imaging (similar to ultrasound probes scanned in 2D to perform 3D imaging) making coregistration difficult, and (iii) patient movement during imaging can generate inaccurate coregistered images, and in turn 3D tomographic images. The possible solutions to overcome these challenges include: (i) developing careful operation procedures and operator training will be developed in order to obtain good quality images using our hand-held based optical imager, (ii) using a tissue conforming garment to aid in standardizing imaging procedures, over imaging directly onto the soft tissue, and (iii) implementing a second tracking system in order to minimize misaligned coregistration issues associated with motion artifact (i.e., subject movements). Along with these ongoing efforts toward clinical translation of the technology, the computational efficiency of generating an automated coregistered image (in near to real time) is parallely improved.

Currently, the OIL is developing a second generation hand-held probe with a smooth curvature based probe head design such that it can better contour to curved tissue, as opposed to the current hand-held probe that has a three-piece segmented feature of flexing. All these advancements in the area of hand-held based optical imagers will empower clinicians to perform real-time coregistered optical imaging onsite using a portable imaging device (similar to ultrasound) toward initial assessments of the tissue, followed by extensive tomographic analysis toward 3D tissue characterization and tumor localization.

ACKNOWLEDGMENTS

The authors would like to thank partial funding support by Imaging Diagnostic Systems Inc. (Fort Lauderdale, FL) for OIL development. Other funding support include Coulter's Young Inventor Award from the Department of Biomedical Engineering, FIU and Pre-Doctoral Presidential Fellowship, FIU.

APPENDIX: AEKF ALGORITHM FOR 3D IMAGE RECONSTRUCTIONS

A modified version[17,40] of the AEKF algorithm[18] was used to perform the 3D image reconstructions. The method of the AEKF algorithm is given by the following pseudocode:

iterate

1: $\mathbf{x}=f(\mathbf{y})$

for $i=1$ to # source illuminations

2: $\mathbf{J}_i=\dfrac{\partial \mathbf{x}_i}{\partial \mathbf{y}}$

3: $\mathbf{K}_i=\mathbf{P}\cdot\mathbf{J}_i^{\mathrm{T}}\cdot(\mathbf{R}_i+\mathbf{Q}_i+\mathbf{J}_i\cdot\mathbf{P}\cdot\mathbf{J}_i^{\mathrm{T}})^{-1}$

4: $\Delta\mathbf{y}_i=\mathbf{K}_i\cdot(\mathbf{z}_i-\mathbf{x}_i)$

5: $\mathbf{P} \leftarrow \mathbf{P} - \mathbf{K}_i \cdot \mathbf{J}_i \cdot \mathbf{P}$
end
6: $\mathbf{y} \leftarrow \mathbf{y} + \Sigma \Delta \mathbf{y}_i$
until convergence

The parameter **x** represents the distributed predictions of the referenced measurements in terms of the logarithm of ac and the phase shift, which are generated by the forward simulator f. The parameter **y** represents the vector of current estimates of the unknown optical property, which is an inverse pseudo-β transform[39] of the optical absorption coefficient due to the fluorophore (μ_{axf}). The measurement error covariance was assumed uncorrelated, and repeated observations (in this case, five) at each detector location were used to experimentally determine the variance for each source-detector pair. The model error covariance **Q** is difficult to estimate for unknown domains and was empirically chosen to be one-fourth the mean of the measurement error variance. The gain matrix **K** for each point illumination i was determined using the measurement error covariance **R**, the model error covariance **Q**, the parameter error covariance **P**, and the Jacobian matrix **J**. The subscript i is used to indicate that the vector or matrix contains only data associated with the illumination source i. The gain matrix **K** is used to update the unknown optical parameter **y** and the parameter error covariance **P**. An initial variance estimate was set to 0.01 for this case and the parameter error was assumed uncorrelated with the initial estimate. While the pseudocode shows **P** as a covariance matrix, in this implementation, only the variances (diagonal elements of **P**) were actually stored and manipulated. The inversion algorithm used here differs slightly from the AEKF (as reported previously)[18] in that it is more computationally efficient. Preliminary studies indicate that the modified algorithm has the same or greater accuracy as the original AEKF algorithm.[40] Additionally, simultaneous multiple point sources as implemented in the hand-held probe design were taken into account in the inverse algorithm during 3D image reconstructions.[4]

[1] B. J. Tromberg, A. Cerussi, N. Shah, M. Compton, A. Durkin, D. Hsiang, J. Butler, and R. Mehta, Breast Cancer Res. Treat. **7**, 279 (2005).
[2] K. S. No and P. H. Chou, IEEE Trans. Circuits Syst., I: Regul. Pap. **52**, 2672 (2005).
[3] B. Jayachandran, J. Ge, S. Regalado, and A. Godavarty, J. Biomed. Opt. **12**, 054014 (2007).
[4] J. Ge, B. Zhu, S. Regalado, and A. Godavarty, Med. Phys. **35**, 3354 (2008).
[5] S. J. Erickson and A. Godavarty, Med. Eng. Phys. **31**, 495 (2009).
[6] N. Shah, A. E. Cerussi, D. Jakubowski, D. Hsiang, J. Butler, and B. J. Tromberg, J. Biomed. Opt. **9**, 534 (2004).
[7] A. Cerussi, N. Shah, D. Hsiang, A. Durkin, J. Butler, and B. J. Tromberg, J. Biomed. Opt. **11**, 044005 (2006).
[8] A. Cerussi, D. Hsiang, N. Shah, R. Mehta, A. Durkin, J. Butler, and B. J. Tromberg, Proc. Natl. Acad. Sci. U.S.A. **104**, 4014 (2007).
[9] K. S. No, Q. Xie, P. H. Chou, R. Kwong, A. Cerussi, and B. J. Tromberg, *Proceedings of the 50th IEEE International Midwest Sym. Circuits Syst.*, ■ (MWSCAS, Montreal, 2007).
[10] B. Chance, S. Nioka, J. Zhang, E. F. Conant, E. Hwang, S. Briest, S. G. Orel, M. D. Schnall, and B. J. Czerniecki, Acad. Radiol. **12**, 925 (2005).
[11] B. Chance, Z. Zhao, S. Wen, and Y. Chen, Rev. Sci. Instrum. **77**, 064301 (2006).
[12] J. R. X. Xu, B. Qiang, J. J. Mao, and S. P. Povoski, Appl. Opt. **46**, 7442 (2007).
[13] T. Durduran, R. Choe, G. Yu, C. Zhou, J. C. Tchou, B. J. Czerniecki, and A. G. Yodh, Opt. Lett. **30**, 2915 (2005).
[14] N. G. Chen, P. Guo, S. Yan, D. Piao, and Q. Zhu, Appl. Opt. **40**, 6367 (2001).
[15] Q. Zhu, E. B. Cronin, A. A. Currier, H. S. Vine, M. Huang, N. G. Chen, and C. Xu, Radiology **237**, 57 (2005).
[16] Q. Zhu, S. H. Kurtzman, P. Hegde, S. Tannenbaum, M. Kane, M. Huang, N. G. Chen, B. Jagjivan, and K. Zarfos, Neoplasia **7**, 263 (2005).
[17] A. Godavarty, M. J. Eppstein, C. Y. Zhang, S. Theru, A. B. Thompson, M. Gurfinkel, and E. M. Sevick-Muraca, Phys. Med. Biol. **48**, 1701 (2003).
[18] M. J. Eppstein, D. J. Hawrysz, A. Godavarty, and E. M. Sevick-Muraca, Proc. Natl. Acad. Sci., U.S.A. **99**, 9619 (2002).
[19] D. S. Kepshire, S. C. Davis, H. Dehghani, K. D. Paulsen, and B. W. Pogue, Appl. Opt. **46**, 1669 (2007).
[20] K. Soléakhéna, D. G. Giancarlo, G. Giovanni, S. Fabio, D. Diego, G. Girolamo, C. Claudio, P. Roberto, L. Jean-Albert, and M. Bruno, Magn. Reson. Imaging **25**, 883 (2007).
[21] D. Shen, D. Liu, Z. Cao, P. D. Acton, and R. Zhou, Mol. Imaging Biol. **9**, 24 (2007).
[22] P. A. Causer, C. A. Piron, R. A. Jong, and D. B. Plewes, AJR, Am. J. Roentgenol. **191**, 1203 (2008).
[23] S. L. Meeks, W. A. Tome, and L. G. Bouchet, *Intensity-Modulated Radiation Therapy: The State of the Art*, (Medical Physics, Madison, WI, 2003).
[24] I. N. Bankman, *Handbook of Medical Imaging*, 1st ed. (Academic, New York, 2000).
[25] P. Bruners, T. Penzkofer, M. Nagel, R. Elfring, N. Gronloh, T. Schmitz-Rode, R. W. Günther, and A. H. Mahnken, Eur. Radiol. **19**, 990 (2009).
[26] E. B. Levy, H. Zhang, D. Lindisch, B. J. Wood, and K. Cleary, J. Vasc. Interv. Radiol. **18**, 303 (2007).
[27] N. D. Glossop, J. Bone Jt. Surg., Am. Vol. **91**, 23 (2009).
[28] M. Nagel, M. Hoheisel, U. Bill, K. Klingenbeck-Regn, W. A. Kalender, and R. Petzold, Proc. SPIE **6918**, 69180G (2008).
[29] H. Zhang, F. Banovac, R. Lin, N. Glossop, B. J. Wood, D. Lindisch, E. Levy, and K. Cleary, Comput. Aided Surg. **11**, 127 (2006).
[30] B. J. Wood, H. Zhang, A. Durrani, N. Glossop, S. Ranjan, D. Lindisch, E. Levy, F. Banovac, J. Borgert, S. Krueger, J. Kruecker, A. Viswanathan, and K. Cleary, J. Vasc. Interv. Radiol. **16**, 493 (2005).
[31] A. Z. Kyme, V. W. Zhou, S. R. Meikle, and R. R. Fulton, Phys. Med. Biol. **53**, 2651 (2008).
[32] A. G. Weisenberger, S. S. Gleason, J. Goddard, B. Kross, S. Majewski, S. R. Meikle, M. J. Paulus, M. Pomper, V. Popov, M. F. Smith, B. L. Welch, and R. Wojcik, IEEE Trans. Nucl. Sci. **52**, 638 (2005).
[33] H. Herzog, L. Tellmann, R. Fulton, I. Stangier, E. R. Kops, K. Bente, C. Boy, R. Hurlemann, and U. Pietrzyk, J. Nucl. Med. **46**, 1059 (2005).
[34] J. S. Goddard, S. S. Gleason, M. J. Paulus, S. Majewski, V. Popov, M. Smith, A. Weisenberger, B. Welch, and R. Wojcik, NSS Conference Record, IEEE, 2002.
[35] C. Whalen, E. L. Maclin, M. Fabiani, and G. Gratton, Hum. Brain Mapp. **29**, 1288 (2008).
[36] M. Koch, J. S. Maltz, S. J. Belongie, B. Gangadharan, S. Bose, H. Shukla, and A. R. Bani-Hashemi, Med. Phys. **35**, 4513 (2008).
[37] D. Hsiang, N. Shah, H. Yu, M. Y. Su, A. Cerussi, J. Butler, C. Baick, R. Mehta, O. Nalcioglu, and B. Tromberg, Technol. Cancer Res. Treat. **4**, 549 (2005).
[38] A. Krol, M. Z. Unlu, K. G. Baum, J. A. Mandel, W. Lee, I. I. Coman, E. D. Lipson, and D. H. Feiglin, Phys. Med. **21**, 39 (2006).
[39] M. J. Eppstein, D. E. Dougherty, T. L. Troy, and E. M. Sevick-Muraca, Appl. Opt. **38**, 2138 (1999).
[40] C. Zhang, M. J. Eppstein, A. Godavarty, and E. M. Sevick-Muraca, Proc. SPIE **4955**, 591 (2003).

AQ: #5 AQ: #6 AQ: #7 AQ: #8 AQ: #9 AQ: #10 AQ: #11 AQ: #12

AUTHOR QUERIES — 026912RSI

#1 Au: Please check changes in sentence “For our optical imaging…” if your meaning was preserved.
#2 Au: Please check changes in sentence “The tracking system can…” if your meaning was preserved.
#3 Au: Please check change of “submersed” to “submerged” in sentence “The phantom was…” if your meaning was preserved.
#4 Au: There are only 42 references in the paper. Please check change of citations to Reference 44 and 45 to Reference 42.
#5 Au: Please verify that the volume should be ″7″ not ″1″ in Ref. 1.
#6 Au: Please verify that the first author should be ″Chou″ not ″No″ in Ref. 2.
#7 Au: Please provide year in Reference 9.
#8 Au: Reference 18 and 41 are the same. Please check deletion of Reference 41 and Renumbering of the references.
#9 Au: Reference 19 and 39 are the same. Please check deletion of Reference 39 and renumbering of References 40–42.
#10 Au: Please verify that the first author should be ″Ken″ not ″Soléakhéna″ in Ref. 20.
#11 Au: Please check changes in Reference 23.
#12 Au: Please verify page number in Reference 28